

## Chapter 6 - Transport Results

### 6.1 Summary

Several models and numerical techniques are used to obtain results for radionuclide transport in the saturated zone. First, a technique based on numerical convolution is developed to link the unsaturated-zone breakthrough curves at the water table to the saturated-zone transport system. In this method, the inputs are the mass flux of radionuclide reaching the water table versus time, along with a generic breakthrough curve in the saturated zone, computed as the response at a downstream location to a constant injection of radionuclide at the footprint of the proposed repository. The numerical implementation of the method was verified by performing a full calculation using the actual time-varying input from an unsaturated-zone calculation as input to the saturated-zone model. The method allows a variety of input flux curves to be computed quickly without recomputing the saturated-zone calculation each time. Assumptions inherent to the convolution technique include steady-state flow and linear transport processes, which, for sorption, implies that the linear-sorption isotherm model must be used. The linear- $K_d$  sorption model is not overly restrictive because one can select a  $K_d$  value that conservatively bounds the sorption behavior predicted by a nonlinear-sorption isotherm model.

Before proceeding to more complex site-specific models, we present a simplified three-dimensional flow and transport model to examine the importance of several transport parameters that are difficult to investigate fully with the current site-scale models. Dispersivity is established as one of the key uncertain parameters that influence the concentration (and hence dose) at accessible environment compliance points. The transverse dispersivity is actually a more sensitive parameter for dilution because it governs the degree of lateral spreading of the plume. Matrix diffusion, established as a valid process in the field test of Reimus and Turin (1997), affects the breakthrough times at a downstream location but, to a first approximation, does not influence the peak concentration. Another important factor regarding matrix diffusion is that it allows

radionuclides to contact minerals in the rock matrix that potentially sorb radionuclides. Even small amounts of sorption have a large effect on breakthrough times and peak concentrations. Finally, this simplified model was used to illustrate that the saturated-zone transport system has the ability to dilute spikes of high concentration and short duration that come from bypassing of the unsaturated zone through fractures. Thus, the saturated zone provides an important component in a "defense-in-depth" strategy in which uncertainties leading to poor performance in one part of the repository system are mitigated by the performance of another radionuclide transport barrier.

To simulate radionuclide transport from the footprint of the repository to a 5-km compliance point, we used a subsite-scale model developed at Sandia National Laboratories (Ho et al., 1996). This model was chosen as an appropriate substitute to performing these calculations using the site-scale model because of the more accurate representation of the geology near Yucca Mountain. When the site-scale model is revised to use the new hydrostratigraphic data based on a 250 x 250-m geologic grid, all calculations will be performed with the site-scale model itself. The subsite-scale model flow results capture the large hydraulic gradient and flow through the geologic strata of relevance downstream of the repository footprint, including the Prow Pass, Bullfrog, and Tram Tuffs units. Radionuclides travel to the east and south from the footprint to a 5-km compliance point. Releases into the Prow Pass unit travel in a more easterly direction than releases in the other units; releases into the Tram unit at the south end of the footprint travel almost due south. All releases follow the dipping stratigraphy, indicating downward movement of radionuclides. This effect may be important if upcoming field studies reveal more reducing conditions with depth, because sorption coefficients of  $^{99}\text{Tc}$  and  $^{237}\text{Np}$  are likely to be much higher and solubilities much lower under reducing conditions.

Transport times to a hypothetical 5-km compliance point under conditions in which the effective porosity is the matrix porosity are on the order of a few thousand years; much shorter transport times result from an assumption of less matrix diffusion. However, the extent of matrix diffusion itself only influences the arrival time rather than the concentration at the downstream

location. This effect is in contrast to differences in fluid flux that may occur due to future wetter climates, which result in earlier travel times but also lower concentrations (greater dilution).

Sorption of radionuclides such as  $^{237}\text{Np}$  onto zeolitic tuffs in the saturated zone also leads to significant retardation and longer travel times to the 5-km compliance point.

The results of the subsite-scale model are then used as input to transport calculations to a hypothetical 20-km compliance point in the site-scale model. Simulations assuming both fracture-like and matrix-like effective porosities in the fractured tuff were performed to investigate the importance of this parameter. In both simulations, the alluvium present along the transport pathways were assigned high porosity. In this set of calculations, the nature of transport in the fractured tuffs is less important as the system becomes increasingly dominated by long predicted travel times in the alluvium. Thus, even if the tuffs are presumed to have a low effective porosity, travel times of 10 ky or more are predicted in the alluvium alone. Furthermore, we show that even small amounts of sorption in the alluvium shift travel times to values on the order of 50 ky, and predicted concentrations at the compliance point are lower than in the absence of sorption. Clearly, for more distant compliance points, the flow and transport behavior of the alluvium becomes increasingly the controlling factor in saturated-zone performance.

The influence of repository heat on saturated-zone flow and transport of radionuclides is also studied using the subsite-scale model. Repository waste heat creates a zone of higher-than-ambient temperature that extends vertically into the saturated zone and along the prevailing flow pathway from the repository. However, the predicted impact on transport of  $^{99}\text{Tc}$  to the 5-km compliance point is very small. One outstanding issue related to repository heat is the possibility of temporary or durable changes to the permeability and porosity due to temperature-dependent rock-water interactions. If these effects turn out to be minor, then we can conclude that repository waste heat has minimal influence on the migration of radionuclides through the saturated zone.

Integrated transport predictions are presented in which we link the unsaturated-zone transport model of Robinson et al. (1997) with the subsite-scale model developed in the present

study to predict the transport of the key radionuclides  $^{99}\text{Tc}$ ,  $^{237}\text{Np}$ , and the isotopes of plutonium. In Robinson et al. (1997), we investigated the performance of the unsaturated-zone system for different infiltration rates that could result from changes to the present-day climate. These predictions of radionuclide mass flux at the water table are input to convolution calculations to predict the combined unsaturated/saturated-zone performance at 5 km. For the unsaturated-zone performance predicted in Robinson et al. (1997), the integrated response in the saturated zone for  $^{237}\text{Np}$  and  $^{99}\text{Tc}$  are a direct consequence of dilution of percolating unsaturated-zone fluid with flowing saturated-zone groundwater. Therefore, poorer predicted unsaturated-zone performance under wetter future-climate scenarios translates directly to higher predicted concentrations in the saturated zone. Sorption onto zeolites in the saturated zone should provide a considerable delay in arrival times for  $^{237}\text{Np}$ . For plutonium, rather than climate change or sorption to the host rock, the key factor influencing concentrations is the propensity of plutonium to sorb to mobile colloids.

Regarding the nature of flow and transport in the fractured tuffs, we experimented with different flow and transport models to investigate different methods of simulating this dual-porosity system. A dual-porosity particle-tracking model for transport was invoked, and the influence of matrix diffusion properties was examined. The results follow those of the matrix-diffusion conceptual model, but several factors argue against its use in large-scale transport model predictions. First, the particle-tracking module does not at present handle the dispersion coefficient tensor formulated as longitudinal and transverse components. Furthermore, although the diffusion model accurately simulates the case of diffusion into an infinite matrix continuum, finite fracture spacings are not part of the model as currently constituted. Therefore, particle tracking cannot be used in site-scale models. A finite-element dual-porosity solution was also investigated. As expected, the dual-porosity flow simulation yielded virtually identical steady-state results to the single-continuum model. Transport results captured well the two extremes (fracture-dominated and pervasive matrix diffusion) but failed to produce accurate results for small but non-negligible diffusion into the rock matrix. We therefore recommend that an appropriate

abstracted transport model employ the effective porosity concept with theoretical relationships involving matrix-diffusion and fracture-spacing parameters used to set the transport porosity throughout the model domain.

## 6.2 Software and Data QA Status

The FEHM code is used to perform all flow and transport calculations in this report. The code is qualified in accordance with Los Alamos quality-assurance (QA) requirements and is documented in several reports by Zyvoloski et al. (1992, 1996b-d). The QA status of the data used in this report is shown in Table 6-1.

<b>Table 6-1. QA Status of Data used in this Chapter</b>			
REFERENCE	QA Status	DTN/ Assession Number	COMMENT
<b>Czarnecki, J. B., et al. 1997.</b> Preliminary three-dimensional finite-element groundwater flow model of the saturated zone, Yucca Mountain, Nevada. USGS YMP milestone number SP23NM3.	non-Q		
<b>Clayton, R. W., et al. 1997.</b> ISM2.0: A 3-D geological framework and integrated site model of Yucca Mountain: Version ISM1.0, Doc ID B00000000-01717-5700-00004, Rev. 0, MOL. 19970122.0053. CRWMS M&O.	Q	MOL. 19970122.0053	By agreement with DOE and NRC, accepted as Q even though it uses some non-Q data.
<b>Zelinski, W. P., and R. W. Clayton. 1996.</b> A 3-D geological framework and integrated site model of Yucca Mountain: Version ISM1.0, Doc ID B00000000-01717-5700-00002, Rev. 1. CRWMS M&O.	non-Q		
<b>Triay, I. R., et al. 1997.</b> Summary report geochemistry/transport laboratory tests. Los Alamos National Laboratory milestone report SP23QM3.	Q	LAIT831341DQ97.003	

## Transport Results

<p><b>Chipera, S. J., et. al. 1997a.</b> Preliminary three-dimensional mineralogical model of Yucca Mountain, Nevada. YMP milestone SP321AM4.</p>	<p>non-Q</p>	<p>No DTN Assigned</p>	
<p><b>Chipera, S. J., et. al. 1997b.</b> Mineralogic variation in drill holes USW NRG-6, NRG-7-7a, SD-7, SD-9, SD-12, and UZ#14: New data from 1996-1997 analysis. Los Alamos National Laboratory YMP deliverable SP321BM4.</p>	<p>Q</p>	<p>LADV831321AQ97.001</p>	
<p><b>Ho, C. K., et al. 1996.</b> Thermo-hydrologic modeling of the potential repository at Yucca Mountain including the effects of heterogeneities and alternative conceptual models of fractured porous media. Level-3 milestone T6536 submitted to U.S. Department of Energy.</p>	<p>Non-Q</p>	<p>No DTN assigned</p>	
<p><b>Triay, I.R., et al. 1996c.</b> Comparison of neptunium sorption results using batch and column techniques: Yucca Mountain Site Characterization Program milestone 3041. Los Alamos National Laboratory report LA-12958-MS.</p>	<p>Q</p>	<p>LAIT831341AQ96.001 LAIT831341AQ96.001 Superseded the initial DTN, LA000000000104.001. DTN Record Accession Numbers: MOL.19970729.0297 MOL.19970729.0298 MOL.19970729.0299 MOL.19970729.0300 MOL.19970729.0301 MOL.19970729.0302 MOL.19970729.0303 MOL.19970729.0304</p>	
<p><b>Triay, I.R., et al. 1996b.</b> Radionuclide sorption in Yucca Mountain tuffs with J-13 well water: Neptunium, uranium, and plutonium: Yucca Mountain Site Characterization Program milestone 3338. Los Alamos National Laboratory report LA-12956-MS.</p>	<p>Q</p>	<p>LAIT831341AQ96.001 DTN Record Accession Numbers: MOL.19970729.0297 MOL.19970729.0298 MOL.19970729.0299 MOL.19970729.0300 MOL.19970729.0301 MOL.19970729.0302 MOL.19970729.0303 MOL.19970729.0304</p>	

### 6.3 Convolution Method for Linking the UZ and SZ Models

---

The time scales of the various transport processes, starting at the drift scale and ending at the accessible environment, play a critical role in the determination of the important parameters and processes, as well as the methods used to predict concentrations and doses. In this section, we present an approximate method for computing concentration and dose at the accessible environment that uses the generic saturated-zone transport calculations as a basis. To perform the calculations of peak concentration at the downstream location, we assume that numerical convolution can be applied to the unsaturated-zone breakthrough curves at the water table using the generic saturated-zone breakthrough curves as the convolution function. The underlying assumptions in using convolution are:

- the transport processes and flow fields from the unsaturated-zone and saturated-zone models are independent of one another;
- the transport processes in the saturated-zone model are linear; and
- steady-state flow is a good assumption for the saturated-zone model.

For sorption, the second assumption implies that the linear-sorption isotherm model must be used. The linear- $K_d$  sorption model is not overly restrictive because one can select a  $K_d$  value that conservatively bounds the sorption behavior predicted by a nonlinear-sorption isotherm model. Regarding steady-state flow, this assumption is a starting point for examining the behavior of the saturated-zone transport system that will be examined in future studies through sensitivity analyses using fully transient flow and transport models.

The convolution integral is the starting point for the coupling of the two models:

$$C_{SZ}(t) = \int_0^t C_{UZ}(t-t')f_{SZ}(t')dt' \quad , \quad (\text{Eq. 6-1})$$

where  $C_{SZ}(t)$  is the concentration at any location in the saturated zone,  $C_{UZ}(t)$  is the time-depen-

dent source concentration from the unsaturated-zone model immediately after entering the saturated zone, and  $f_{SZ}(t')$  is the residence-time distribution function for the saturated zone at the location where  $C_{SZ}(t)$  is being calculated. The latter term is computed from the response curve in the saturated zone to a pulse input of solute at the position the radionuclides enter the saturated-zone model. Equation 6-1 is not the most straightforward form for coupling the models, because the unsaturated-zone source term is actually most conveniently expressed as the time-dependent mass flux  $\dot{m}_{UZ}(t)$  entering the saturated zone. This problem is circumvented by rewriting the convolution integral as follows:

$$C_{SZ}(t) = \int_0^t \dot{m}_{UZ}(t-t') \frac{\bar{C}_{SZ}(t')}{m_p} dt' \quad , \quad (\text{Eq. 6-2})$$

where  $\bar{C}_{SZ}(t')$  is the downstream concentration-time response curve to the tracer pulse of mass  $m_p$ . The generic curves representing saturated-zone transport are actually the responses to a constant mass flux rather than a pulse but are easily differentiated numerically during implementation to obtain  $\bar{C}_{SZ}(t')$  before applying the convolution method.

### 6.4 Simplified Three-Dimensional Flow and Transport Results

---

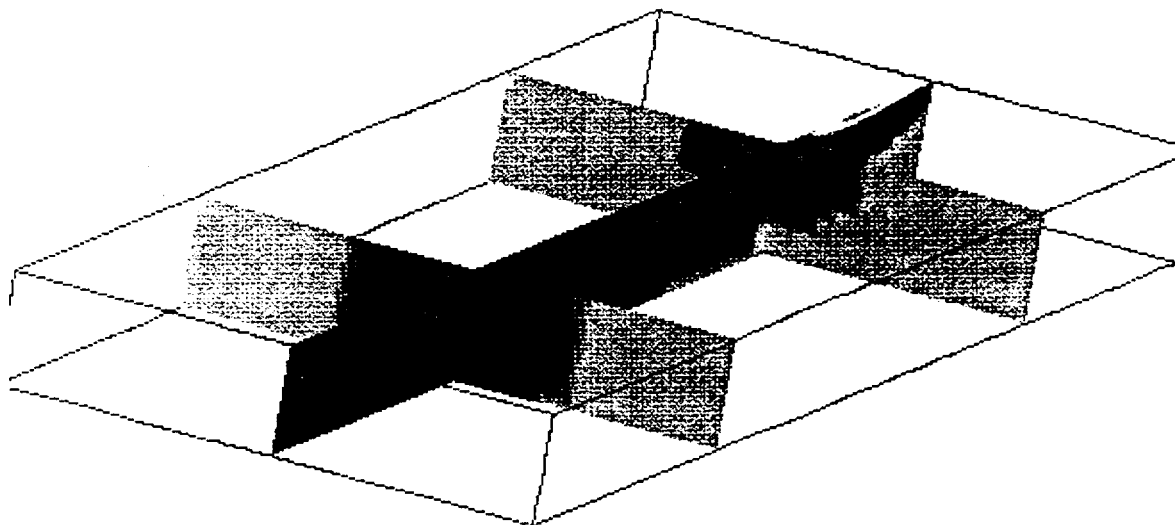
To illustrate the role of transport processes such as dispersion, sorption, and matrix diffusion on the performance of the saturated zone, we present a generic transport simulation to demonstrate the nature of the dispersion process and the time scales involved. We then use the results in an approximate method based on the convolution integral for computing concentration versus time at various locations. For these simulations, the radionuclide source term used is from the August, 1996, unsaturated-zone modeling study (Robinson et al., 1996). This section is designed to illustrate the behavior of the system under idealized conditions. Integrated transport

calculations using the more recent unsaturated-zone transport model of Robinson et al. (1997) are presented in Section 6.13.

In this section, we assume a constant radionuclide flux entering the top of the model in the area defined by the footprint of the potential repository, that is, the projection of the repository vertically down to the water-table surface. Although more complex distributed mass flux patterns at the water table are possible, it is premature to study this aspect of the coupled unsaturated/saturated-zone transport system. In contrast to the typical "dilution factor" approach used in many studies, in the present study, radionuclide mass flux from the unsaturated-zone model is used directly as input to the saturated-zone model. The key advective parameter controlling dilution is the saturated-zone fluid velocity, which, when combined with the unsaturated-zone radionuclide mass flux, yields a concentration prediction within the saturated zone. Furthermore, the concept of a "mixing depth," in which radionuclide is assumed to be confined to a given thickness, is not employed. Instead, radionuclides are mixed in a very thin patch of computational cells (about one meter thick in the vertical direction) at the repository footprint and allowed to spread by dispersion during transport to the downstream location. The dispersion parameters used in the simulations control the degree of lateral and longitudinal spreading for this idealized set of simulations. Later in this chapter, we present calculations using the subsite-scale and site-scale models in which strata of contrasting permeability values also control the plume migration.

To generate a model result, transport is simulated until a steady-state concentration profile is achieved, approximated as two times the mean travel time for the 25-km distance. Figure 6-1 is a three-dimensional representation of the steady-state solute plume for the 250-m dispersivity case. A well-defined plume initiating beneath the potential repository spreads in both the longitudinal (north-south) and transverse (east-west and vertical) directions, resulting in lower concentrations at downstream locations.

Because peak dose depends on the concentration present at a location downstream from the site, dispersion will play a key role in the resulting dose calculation. Figure 6-2 shows the



**Normalized Concentration**



**Figure 6-1.** Radionuclide plume after long-term injection at the idealized repository footprint. Dispersivity: longitudinal - 250 m; transverse - 25 m.

concentration history during the simulation directly beneath the potential repository and at the water table at a 25-km distance. First, note the normalized concentration values at the plateaus for the two curves. These values are directly related to the radionuclide concentration and hence peak dose. At a given dispersivity value, increasing the assumed distance to the accessible environment from 0 to 25 km reduces the concentration by a factor of roughly 12. The concentration directly beneath the potential repository reflects the mixing of contaminated unsaturated-zone fluid with saturated-zone water before dispersion, matrix diffusion, or sorption affect the plume. The twelve-fold decrease in concentration at 25 km highlights the importance of the dispersivity and the role of scale in reducing peak dose.

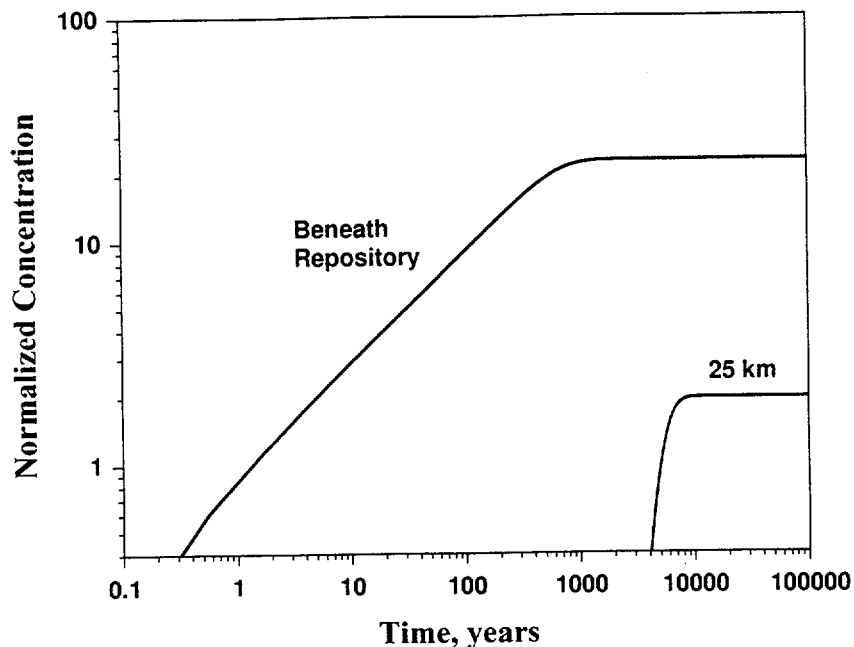


**Figure 6-2.** Normalized concentration responses directly beneath the repository and at the water-table surface 25 km downstream for the plume depicted in Figure 6-1.

There are also gradients in concentration vertically and horizontally at a given location due to the spreading of solute via a transverse dispersion mechanism. Figure 6-3 compares the influence of longitudinal and transverse dispersivity in impacting the peak concentration at a downstream location. The two calculations with transverse dispersivity of 10 m yield almost identical results despite the difference in longitudinal dispersivity. This result suggests that transverse dispersion is the critical parameter controlling the peak concentration. Finally, the role of matrix diffusion and sorption on the predicted downstream breakthrough curve is shown in Figure 6-4 (sorption coefficient of 1 cc/g is assumed for the sorption case). In Chapter 5, we showed that, assuming pervasive diffusion into the rock matrix, the saturated-zone system can be simulated using a single-continuum model in which the effective transport porosity is controlled by the matrix porosity. To examine the influence of matrix diffusion on performance, we compare two simulations. For the “no matrix diffusion” case, we assume a uniform porosity of  $10^{-4}$ , typical

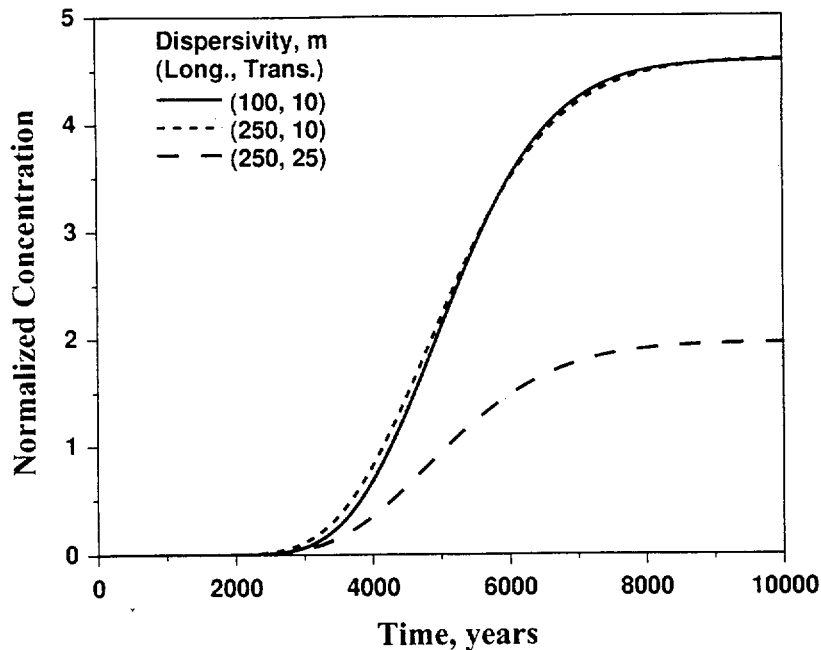


**Figure 6-3.** Influence of longitudinal and transverse dispersivity on the breakthrough curve at the 25-km water-table position.

of the fracture porosity, whereas for the “matrix diffusion” case we assume a porosity of 0.1. The larger porosity suggested by the matrix diffusion increases the breakthrough *time* at the downstream location, but the *concentration* at the plateau of the breakthrough curve is not affected, because this concentration is controlled by dilution and dispersion. Similarly, sorption on the matrix rock provides an additional delay of the breakthrough curve at the downstream location, but the concentration at long times is not affected by sorption.

The influence of these processes on the concentration breakthrough curves for realistic unsaturated-zone transport scenarios is now discussed. This analysis was performed with the results of the unsaturated-zone flow and transport model results of August, 1996, (Robinson et al., 1996) for a uniform percolation, 4-mm/y scenario. Figure 6-5 shows the computed concentration versus time curves at 25 km and directly beneath the potential repository for the various transport cases. The concentration directly beneath the repository (“dilution only”) represents the

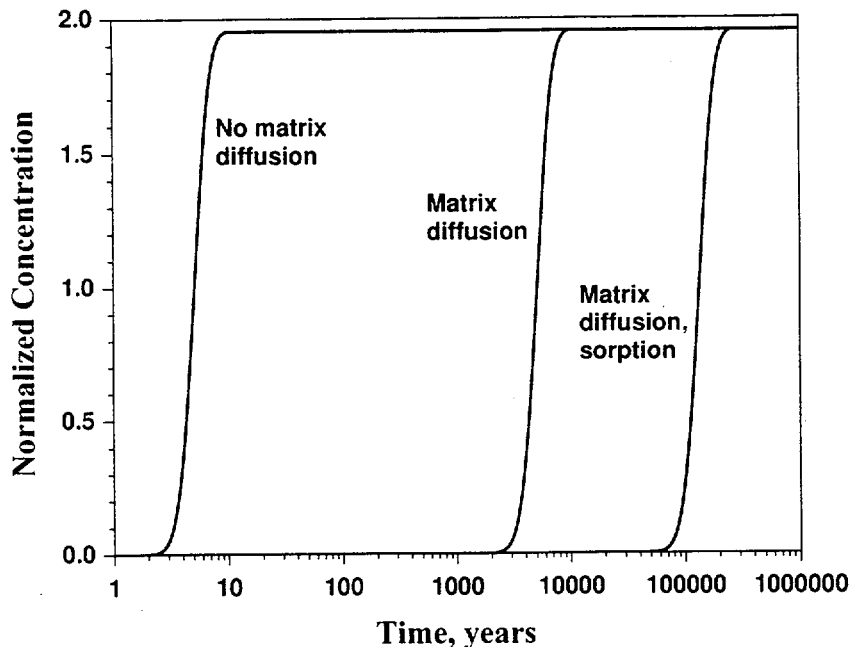


**Figure 6-4.** Influence of matrix diffusion and sorption on the breakthrough curve at the 25-km water-table position.

instantaneous mixing of percolating unsaturated-zone fluid with saturated-zone water. The “dilution, dispersion” case is a downstream concentration breakthrough curve at 25 km, but because the transport time for an effective porosity of  $10^{-4}$  is only 5 y in this simulation, there is likewise virtually no delay due to transport. However, there is additional dilution due to dispersion of the radionuclide. Thus, the effectiveness of dispersion-related dilution is seen by comparing the “dilution only” and “dilution, dispersion” cases.

The third curve, the “dilution, dispersion, matrix diffusion” case, was computed assuming an effective porosity of 0.1 to represent the influence of matrix diffusion in increasing the pore space available for transport. For this idealized system, there is a delay time of the order of 5000 y due to saturated-zone transport, which influences the breakthrough of the earliest arriving radionuclide but has little impact (compared to the low-porosity case) for the bulk of the radionuclide inventory in this simulation.

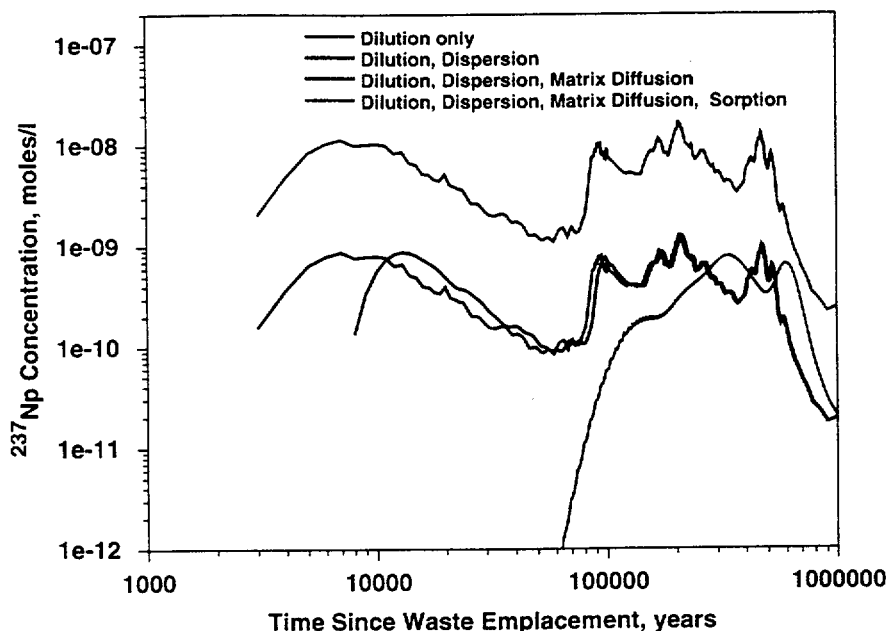


**Figure 6-5.**  $^{237}\text{Np}$  response predicted by numerical convolution for water-table breakthrough curves generated based on the unsaturated-zone transport model. The curves illustrate the influence of various saturated-zone transport processes on predicted concentrations.

Although this result might lead to the conclusion that matrix diffusion itself affects performance only minimally, there are three important reasons why this conclusion is incorrect. First, the regulatory time frame is crucial to the relevance of any portion of the breakthrough curve. Under a 10,000-y regulatory criterion, any component of the system that provides transport times approaching or exceeding 10,000 y will directly benefit performance because of the potential for shifting the mass arrival at the accessible environment to times greater than the compliance time. In these calculations, the saturated zone is shown to provide a time period of several thousand years in the absence of sorption. This time delay could approach 10,000 y in the saturated zone alone under the final predictions of saturated-zone flow and transport and, thus, would be an important barrier in itself. Because the barrier would be essentially independent of the uncertainties in waste package, engineered-barrier system (EBS), and unsaturated-zone performance predictions, the delay time afforded by the saturated-zone transport system would be an important aspect of a

“defense-in-depth” strategy for demonstrating regulatory compliance. Second, if delay times of thousands of years can be demonstrated, dispersive mixing will tend to further dilute any pulse of radionuclides that happens to reach the water table early due to breakdown in performance of the near-field or unsaturated-zone system. This dilution effect is distinct from the normal spreading and dilution at long times, as it is related to the ability of the saturated-zone transport system to smooth out pulses of radionuclides, whereas the dilution mentioned until now is due to bulk mixing of a constant-concentration source at the repository. The final reason that matrix diffusion influences the performance predictions is that it allows radionuclides to contact the sorptive matrix minerals, causing further delays of the breakthrough at the accessible environment. The “dilution, dispersion, matrix diffusion, sorption” curve in Figure 6-5, in which a very slight sorption coefficient of 1 cc/g was assumed, shows considerable delay of the earliest arriving radionuclide and, perhaps more importantly, dilution of the first peak of the breakthrough curve from the unsaturated-zone model. This sorption coefficient is appropriate for key radionuclides such as  $^{237}\text{Np}$  sorption on zeolitic tuffs (Triay et al., 1997).

The ability of the saturated zone to “selectively” influence the peak concentration associated with the portion of the inventory that bypasses the unsaturated-zone natural barrier is perhaps the most important reason that the transport characteristics of the saturated zone are important to total system performance. This point has gone unrecognized in past TSPA analyses. As a rough, qualitative explanation of this process, it may be stated that whenever a spike in elevated radionuclide flux reaches the water table, if the width of that spike (the time duration over which the spike occurs) is of the same order or smaller than the saturated-zone transport time to the accessible environment, then the saturated-zone transport system will “selectively dilute” the spike. This is why the predictions show that the saturated-zone transport processes, such as sorption, have a strong effect on the first peak of the unsaturated-zone breakthrough curves but relatively small influence on the second, widely distributed peak. Past analyses also show that the negative influence on performance of unsaturated-zone fracture flow and transport is mitigated if the engineered barrier or low solubility limits the release rate of radionuclides from the near field.

This behavior is analogous to the ability of the saturated zone to dilute a concentrated spike. A similar result would be obtained from an analysis based on moments of the breakthrough curves from each subsystem (i.e., EBS, unsaturated zone, and saturated zone), but the convolution integral is a convenient way to compute actual breakthrough curves.

There is a good chance that the unsaturated-zone barrier calculations will have a considerable probability of having rapid water-table breakthrough curves for some of the inventory, such that the maximum mass flux will be within the first peak. The saturated-zone transport system will provide a hedge against those performance calculations in which the unsaturated-zone barrier fails. Simply assuming a single dilution factor, rather than considering the details of dilution of a time-varying unsaturated-zone breakthrough curve in the saturated zone, would be overly conservative and unnecessary. A single dilution factor that reduces the concentration by a fixed factor, regardless of the nature of the water-table breakthrough curve, will overestimate the concentration at the accessible environment for sharp pulses of radionuclide entering the water table. The convolution-integral approach is a superior way to couple the models in a way to properly reflect the role of the saturated zone in total system performance.

### **6.5 Rationale for Subsite-Scale Transport Model**

---

Transport calculations using the site-scale flow and transport model being developed in collaboration with the USGS produce results that in some aspects seem unrealistic based on our current conceptualization of the site saturated-zone system. The USGS/Los Alamos current site model is to be considered an interim model that, at present, lacks some of the features needed to perform detailed radionuclide transport predictions. In particular, although the model is calibrated with respect to measured head data, calculations of transport from the repository to the accessible environment are problematic at present due to the coarse grid on which the hydrostratigraphic model was built. Near Yucca Mountain, the geologic structure embodied in this preliminary version of the model (shown in Figure 3-3) does not capture the stratigraphy contained in geologic

models such as ISM 2.0 (Clayton et al., 1997). Therefore, although the model predicts the general direction of flow and transport at the site scale, radionuclides injected at the water table beneath Yucca Mountain do not migrate in what is thought to be a realistic fashion. Once away from the site, the model does capture the prevailing groundwater flow and transport system at an appropriate level of detail and is used to further transport contaminant from the subsite-scale model described in Section 6.4.

To illustrate the behavior predicted by the current site-scale model, tracer of uniform concentration was released to the saturated zone in an area defined by the footprint of the proposed repository. The plume spread slowly throughout the entire depth of the model beneath the source region. The downward spreading of the plume is controlled by the low permeability, upper-volcanic confining unit (UVCU, unit 14), which lies directly downstream from the repository footprint. In the current model, the UVCU extends over much of the depth of the domain and covers about 25% of the width of the domain, as shown in Figure 3-3. This unit creates a permeability barrier that eventually forces the tracer into the higher permeability, lower carbonate aquifer (units 3, 5 and 7), which it then follows in a southwesterly direction. Updating the model stratigraphy with the more refined geologic model shown in Figure 3-4 should alleviate this problem as the UVCU does not reside in the center of the new site stratigraphy. As discussed in Chapter 3, the next version of the flow and transport model will use this updated stratigraphy.

The site geologic model ISM 2.0 (Clayton et al., 1997) was available for use on February 20, 1997, too late to incorporate into the site-scale flow model. The Stratamodel representation of this model, discussed in Section 3.5, is based on the new ISM 2.0 data near Yucca Mountain and is discretized on a 250 x 250-m grid. This revised stratigraphic representation will be incorporated into the flow and transport model in early FY98. However, it was impossible to rebuild and regrid the flow model, recalibrate it, and run transport predictions in time for inclusion in the present study.

A subsite-scale flow model developed by Sandia National Laboratories (Ho et al., 1996) was made available for performing radionuclide transport calculations. This model was originally developed for groundwater travel time calculations carried out in 1995, documented in Altman et al. (1996). That version of the modeling was performed using the STAFF3D code, but since that time, Ho et al. (1996) have developed a nonisothermal version of the model using FEHM in which they examined issues of repository heat and rock-water dissolution/precipitation reactions and their potential influence on saturated-zone flow. In the present study, we use this model to simulate the transport of radionuclides to a hypothetical 5-km accessible environment boundary and to the outer boundary of the model at about 6 km from the repository. We then use this predicted radionuclide mass flux as the input to the site-scale model to carry the radionuclides downstream to a 25-km compliance point. It is anticipated that when the ISM 2.0 geologic model is built into the USGS/ Los Alamos site-scale model, the results near Yucca Mountain will be reproduced, and the transport calculations will be taken to a 20- or 25-km accessible environment compliance point.

### **6.6 The Sandia National Laboratories Subsite-Scale Flow model**

---

The geologic structure incorporated in the subsite-scale model will be reviewed briefly here; for details, see Ho et al. (1996) and Altman et al. (1996). The boundaries of the model domain relative to those of the site-scale model are shown in Figure 6-6. The model boundaries correspond roughly to the Yucca Wash to the north, the Forty Mile Wash to the east, and the Windy Wash fault to the west. The southern boundary was chosen to extend the model far enough to compute pathways at least to 5 km from the potential repository for the groundwater travel time calculations. In the vertical, the model extends 250 m below the water table. In addition, portions of the model extend above the water table so that heat generated from the potential repository can be simulated and its influence on saturated-zone behavior investigated (Ho et al., 1996). In the present study, these heat effects are not included, and the porosity and permeability of this part of the model are set to zero to confine the flow to the saturated zone.

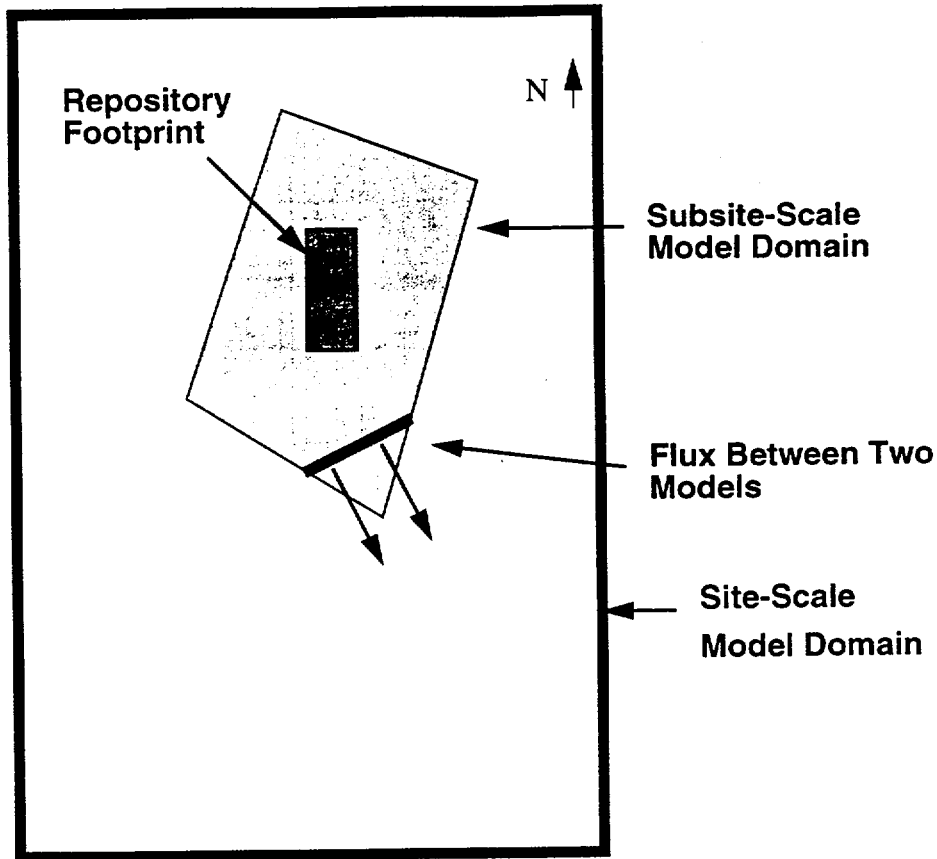


**Figure 6-6.** Placement of the subsite-scale model domain within the site-scale model domain.

The permeability of the hydrogeologic units present at the water table are shown in Figure 6-7. Key features include the contrasts in permeability between the different stratigraphic units as well as the low-permeability zones inserted at faults to simulate the large hydraulic gradient. Underneath the repository, the hydrostratigraphic units present are the Prow Pass in the east and north portion of the footprint, the Bullfrog in the central, and the Tram to the south and east. In addition, a few nodes identified as part of the Solitario Canyon fault zone or splay are projected as being below the footprint. This fact is probably a result of the process of projecting an approximate repository footprint onto a saturated-zone model with insufficient resolution to capture the footprint in detail. Furthermore, because these nodes are assigned low permeability to capture the large hydraulic gradient, the model is inappropriate for investigating potential fast-pathway flow in

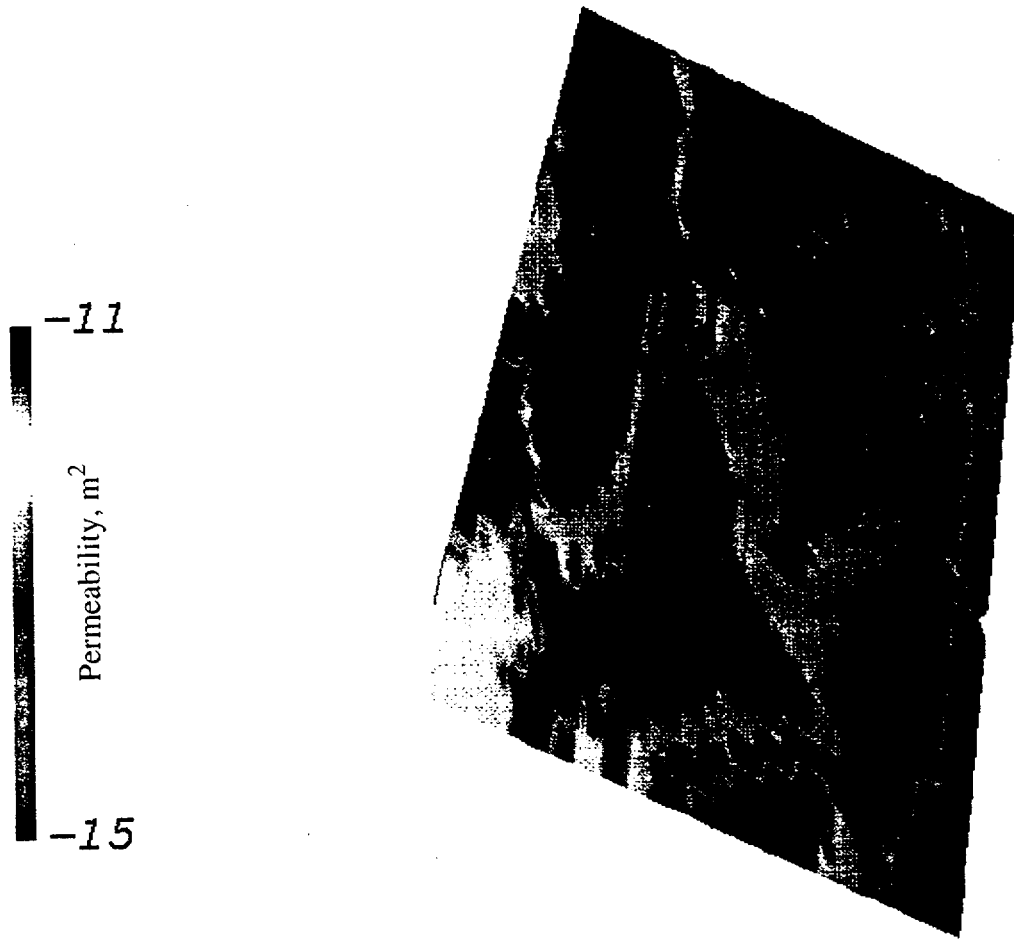


**Figure 6-7.** Permeability distribution of the subsite-scale model at the water table. North is at the top of the figure.

this fault system. Therefore, we will limit our studies to radionuclides reaching the water table in the three hydrostratigraphic units mentioned above, as well as investigate the pathways of the integrated plume of radionuclide over the entire repository footprint. Beneath the water table, the units dip to the east, exerting control over the pathways taken by radionuclides in the saturated zone.

A significant difference between the present study and Altman et al. (1996) is the extent of the potential repository footprint to the east. Altman et al. (1996) used the original SCP repository design in which a portion of the footprint extended to the east of the Ghost Dance fault, bringing some of the Calico Hills formation into play at the water table. They found that particles entering the saturated zone in the low-permeability Calico Hills unit had much longer travel times than those entering the other units. By contrast, in the present study, the Calico Hills is not present at the water table underneath the repository under the current design scenario. This fact implies that under the current design, radionuclides will immediately transport in the saturated zone in the more permeable units.

In the version of the model used in the present study, the top of the water table is modeled as a confined unit in single-phase flow, the bottom surface is a no-flow boundary, and the fluid pressures along the outer boundaries are fixed-pressure boundaries with values derived from Ho et al. (1996). Thus, the modeling approach is equivalent to that used in the site-scale model. The no-flow boundaries at the water table and at depth preclude the simulation of water table rise and limit the extent of vertical flow possible in the simulations. Pressure versus depth along the boundaries was computed based on the weight of the fluid column there and held fixed as well. This method enforces a condition of no vertical flow at the boundaries. In the nonisothermal version of the flow simulation presented below, the temperature at the water table was held fixed at 32°C and the bottom surface was fixed at 40°C. Heat-flux bottom boundary conditions are also possible but were not used in the present study. For the isothermal simulation, the entire system was fixed at a constant temperature of 32°C, and the integrated flux values for the two cases were compared. Both a full heat and mass transfer solution and an isothermal flow solution were computed with FEHM out to long times (steady state), and these solutions were used for subsequent transport simulations. Figure 6-8 shows the computed hydraulic head map (converted from the fluid pressure in the simulation) using the hydrologic property values supplied by Sandia National

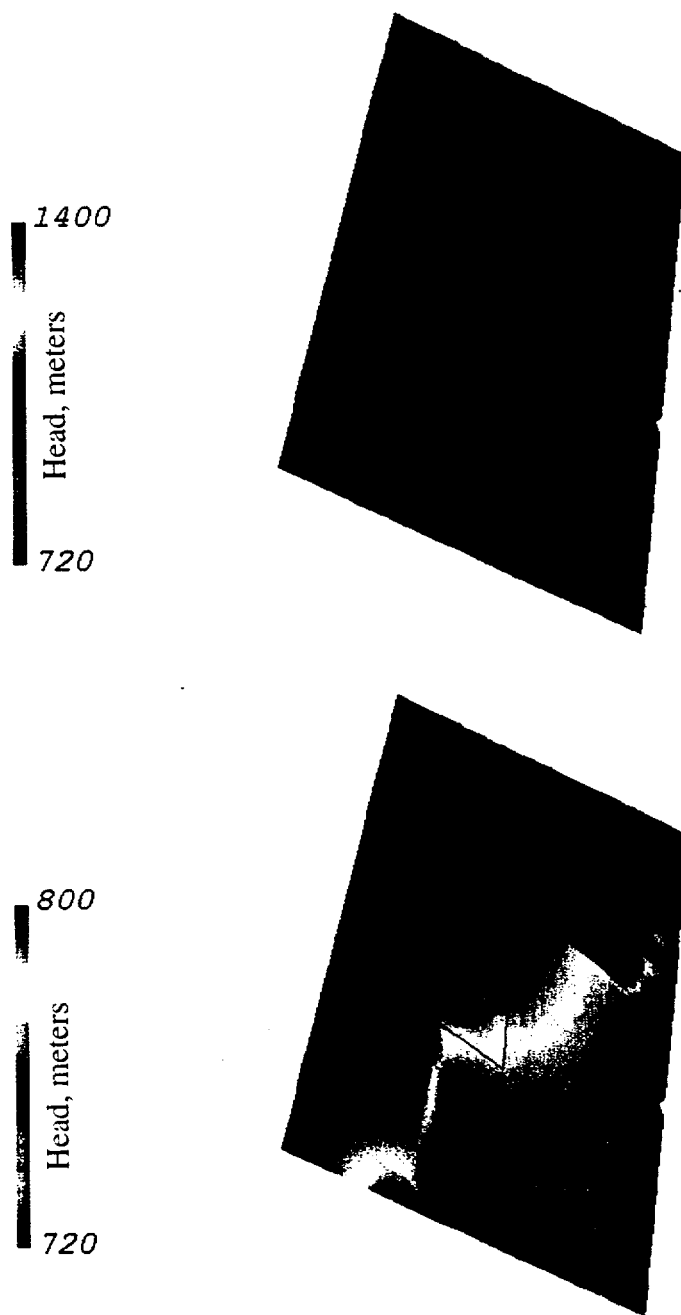


**Figure 6-8.** Predicted head values in the subsite-scale model. Top figure: heads over the entire range of values in the model. Bottom figure: condensed scale from 720 to 800 m to illustrate details in the low-gradient region downstream from the potential repository. North is at the top of the figure.

Laboratories in this version of the model (Ho et al., 1996). The top figure is the head over the entire range of the values, and the bottom figure details the lower range of values downgradient of the repository.

## Transport Results

Table 6-2 lists the permeability and porosity values used in the model simulations. Although a formal parameter-estimation technique was not performed (manual trial-and-error was used instead), the computed head values agree to within 1 m with the measured well data in most places. For a description of the match to the data for the STAFF3D version of this model, see Altman et al. (1996). To obtain the fit, including the large hydraulic gradient, several fault zones in the model were assigned low permeabilities; these values were adjusted to match the data. The fault zones, visible in the permeability map in Figure 6-7, are the Solitario Canyon Fault and associated splays, the Drill Hole Wash structure, and the Yucca Wash structure. Thus, the conceptual model of fault zones as flow barriers is incorporated into this model, thereby resulting

**Table 6-2. Hydrogeologic Layers and Properties for the Subsite-Scale Flow and Transport Model**

Unit	Permeability (m <sup>2</sup> )	Porosity
Topopah Spring welded	5e-12	0.16
Calico Hills	7e-14	0.33
Prow Pass	4.2e-13	0.28
Bullfrog	3.2e-14	0.18
Tram	7e-14	0.22
Lavas	1e-14	0.15
Lithic Ridge tuffs	1e-13	0.16
Solitario Canyon fault gap	5e-14	0.2
Yucca Wash fault	5e-15	0.2
pre-Lithic Ridge tuffs	4.2e-13	0.15
Solitario Canyon fault splay extension	5e-18	0.2
Drill Hole Wash fault	1e-15	0.2
Solitario Canyon fault	1e-15	0.2
Solitario Canyon fault splay	1.e-14	0.2
Tiva Canyon welded	1.7e-12	0.26
PTn	2e-13	0.55

## Transport Results

---

in the large gradients in the locations observed in the head data. Alternatively, perched water could be partially responsible for the (perceived) large gradient. This alternative is not included in the present study but is not anticipated to change the radionuclide transport results significantly. As long as the measured low gradient to the south and east from the repository is reproduced, the details associated with the flow-field upgradient from the site will probably not influence flow and radionuclide migration along the transport pathways to the accessible environment.

In the remainder of this section, we present additional results predicted by the flow model. The next section reports the radionuclide transport results. Figure 6-9 shows the velocity vectors from the model at the water-table surface. Of course, the vectors are in a direction normal to the pressure contours predicted by the model. From the repository footprint, this direction is to the south and east. The relative magnitudes of the vectors are in keeping with the local permeability. For example, velocities are greatest in the Prow Pass unit because of the higher permeability values in this unit. Velocities at greater depth reveal similar features with differences due to the complex stratigraphy represented in the model.

Another aspect of the flow system is the influence of nonisothermal conditions on the flow solution. For this version of the model, it is important to state the limitations of the present analysis. Because the model only extends 250 m below the water table, the carbonate aquifer is not represented. Therefore, the influence of temperature gradients on possible vertical flow between the tuffs and the carbonate aquifer cannot be investigated. Only temperature effects within the upper 250 m will be represented in this model. That having been said, we examine the influence of the approximately 10°C difference in temperature from the top to bottom of the model on the flow simulation results. Visual inspection of velocity vectors yield only very slight differences in the relative magnitudes and directions of flow. The only difference is the magnitude of total fluid flow through the model domain, which is about 10% greater in the nonisothermal model due to the higher temperature and corresponding higher average fluid viscosity. This difference is small compared to other uncertainties in the model. Thus, we perform the transport

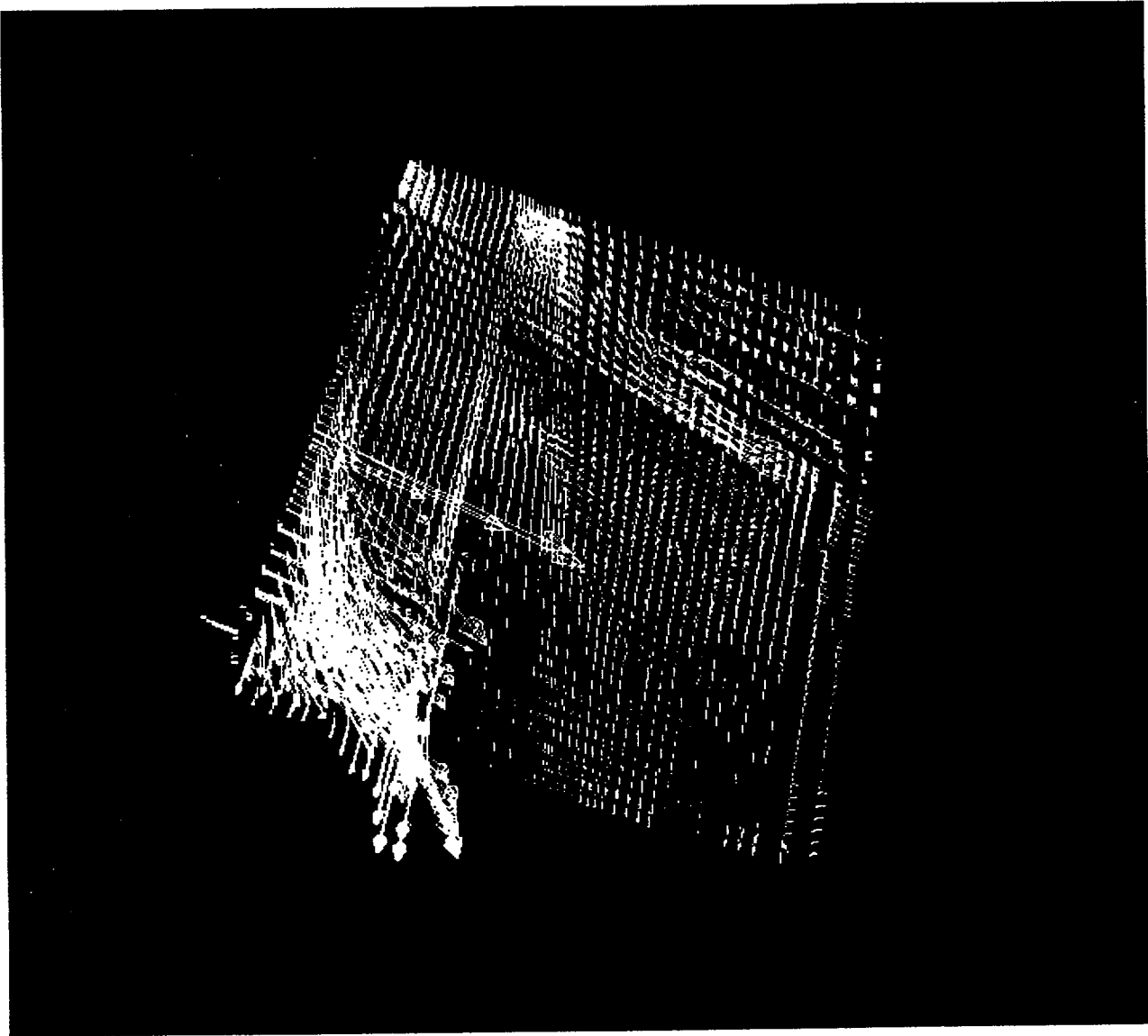


**Figure 6-9.** Three-dimensional velocity vector field predicted with the subsite-scale model. North is at the top of the figure.

simulations in isothermal flow for the remainder of the present study. A re-examination of this issue using the site-scale model is warranted because of the potential for enhanced vertical fluxes between the tuff and carbonate aquifers.

### 6.7 Radionuclide Transport Base-Case Results

---

In this section we present results of radionuclide transport calculations from the footprint of the repository at the water table to a hypothetical 5-km compliance distance. For these calculations, we use the finite-element transport solution option in FEHM. In addition to concentration values, we report results of the cumulative radionuclide mass exiting the subsite-scale model domain versus time. Both of these measures of performance of the saturated zone are important to consider. The concentration at the 5-km distance would be directly related to peak dose at that location. The uncertainty in the exact nature of the regulations requires that various distances be examined. The 5-km distance is taken mainly for historical reasons but also because this model extends far enough for this distance to be examined. For accessible-environment distances of 10 km or more, the larger site-scale model domain must be used. In the future version of that model, calculations from the repository footprint to compliance points as distant as 25 km will be made. However, in this interim report, we examine the total radionuclide mass flux output from the subsite-scale model, regarding it as a mass input to the site-scale model. This “piecing together” of models, though necessary at present, is a temporary measure allowing us to examine the entire transport system to the more likely compliance points 20 km or greater from the repository. The total radionuclide mass flux output from the subsite-scale model is, thus, an intermediate result needed to complete the calculation.

We begin the transport simulations by displaying the predicted radionuclide plume from the repository footprint. For this calculation, we supply a constant mass flux of radionuclide to each node in the footprint for long times and map the plume direction and concentration after 10 ky. For this model, with the porosities given in Table 6-2, the concentrations at all locations are no longer changing significantly with time, and the total radionuclide fluxes into and out of the model are approximately equal. Figure 6-10 shows horizontal slices through the model at the water-table surface and at a depth of 250 m below the water table. The radionuclides migrate to

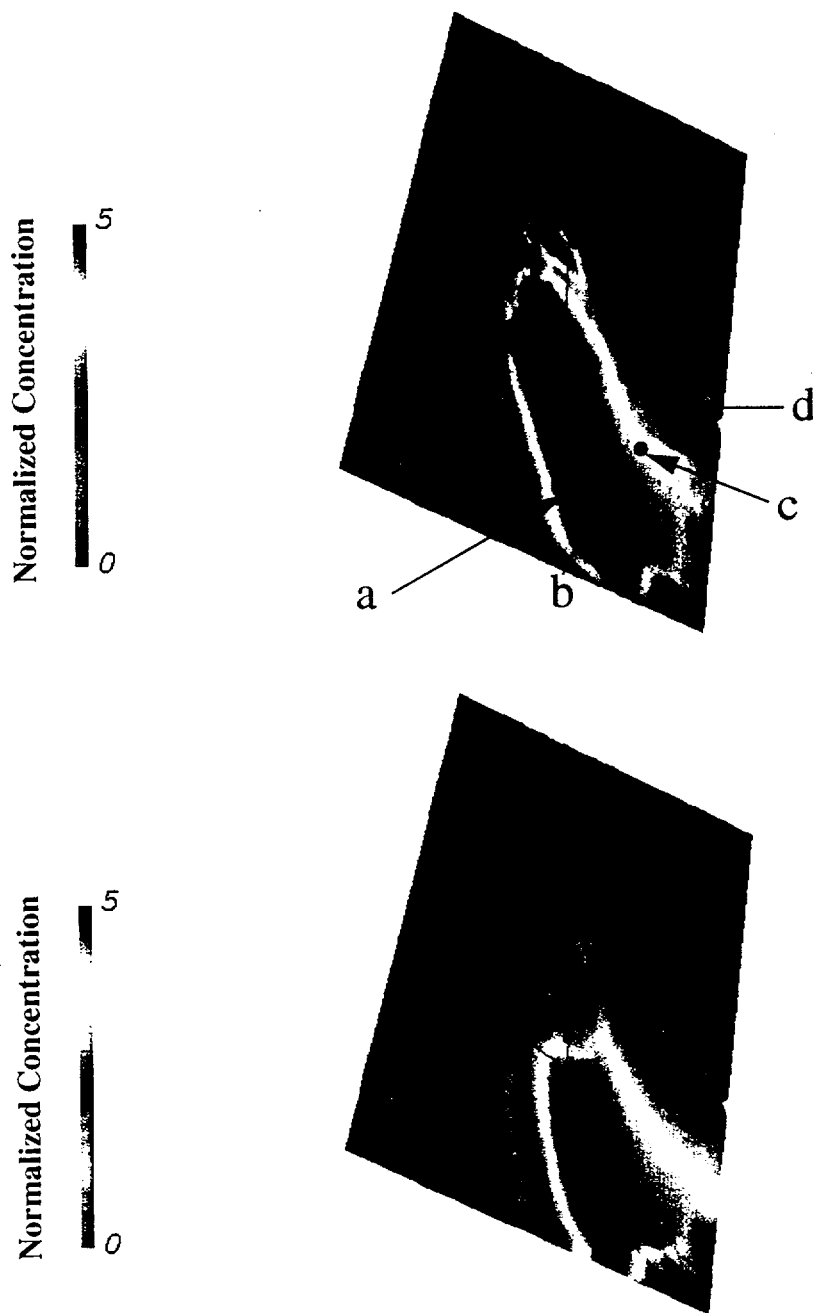


**Figure 6-10.** Radionuclide plume after constant injection at the repository footprint for 10 ky. Top figure: normalized concentration at the water table. Bottom figure: normalized concentration at a 250-m depth. The labeled points identified in the top figure are located 5 km from the southeast corner of the repository footprint. North is at the top of the figure.

the south and east from the repository footprint, as expected from the pressure and velocity distributions presented earlier.

## Transport Results

---

In addition to this horizontal migration, significant vertical movement is predicted, as evidenced by the similarity of the concentration contour plot at greater depth. Although there is apt to be some numerical dispersion and smearing of the concentration front in the vertical direction due to the 50-m grid spacing in this direction, there is also apparent vertical dispersion caused by the hydrostratigraphic framework built into the model. Because the layers dip to the east and the water table is relatively flat, local flow directions are down-dip within permeable layers, such as the Prow Pass unit, as well as to the east and south. The result is a vertical spreading of the radionuclide plume. For this system, as long as there are permeability contrasts of an order of magnitude or greater, the flow and transport will be predicted to be effectively strata-bound, resulting in significant downward plume migration from the repository footprint.

Given this general flow direction, we selected the four positions shown as black dots in the upper plot of Figure 6-10 as the hypothetical 5-km compliance points, that is, this distance as measured from the southeast corner of the repository. The concentration versus time response at the water table at each of these points is shown in Figure 6-11. At this point, the concentration values are arbitrary, because they are based on a radionuclide mass flux of 1 mol/s at each of the 145 nodes on the footprint, but they can be compared to each other and illustrate the transport time-scale predicted by the model. Mean arrival times are on the order of 2000 years, with the most rapid arrival predicted at position b. This position is also the one where the plume reaches the highest concentration plateau, suggesting that the direction from the footprint to position b is the approximate overall direction of the plume and, thus, the location where the maximum concentrations will be experienced. For this reason, in many of the subsequent sensitivity analyses, we use position b as the position for examining the concentration breakthrough curves, calling it the "5-km center-of-mass location."

To examine the extent of vertical spreading of the plume, we plot in Figure 6-12 the concentration-time response for various depths at the 5-km center-of-mass location (position b). The red curve is the breakthrough at the water table, and the other curves are values at increasing depths. There is little variation in the predicted concentration response with depth by the time the

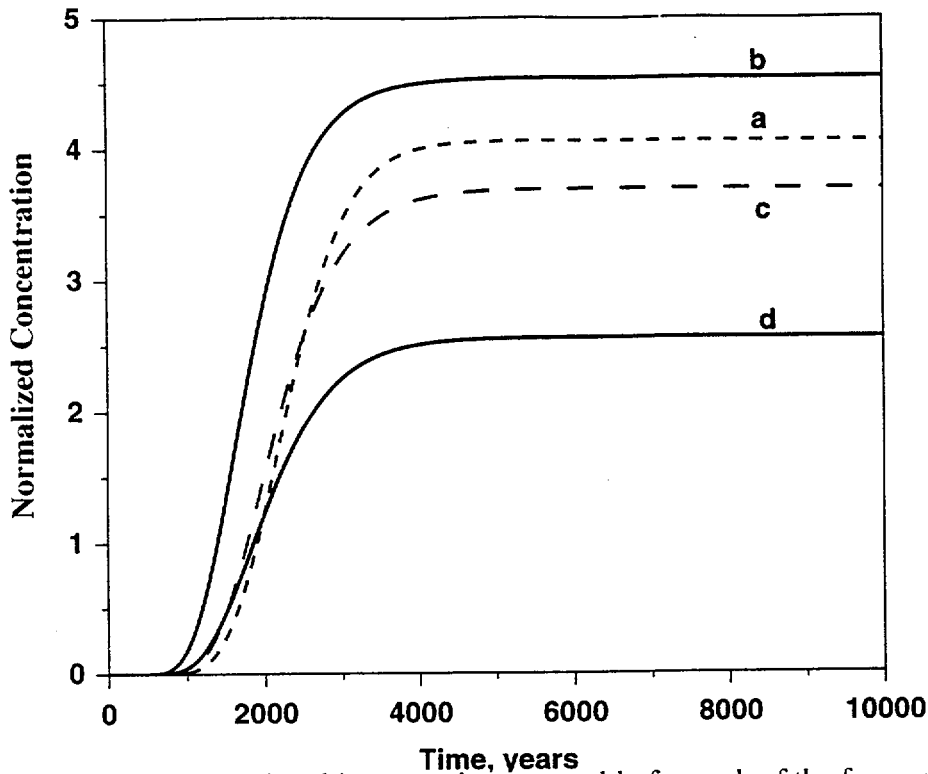


**Figure 6-11.** Concentration time history at the water table for each of the four points identified in Figure 6-10. The curve labels refer to the 5-km compliance points identified in Figure 6-10.

plume reaches this position 5 km from the footprint. Strata-induced vertical dispersion certainly accounts for some of this behavior, although we believe there is also numerical dispersion smearing the results. We anticipate that this investigation will be undertaken using the next version of the site-scale model with its enhanced resolution of the hydrostratigraphy and further grid refinement in the location of the radionuclide plume. We, therefore, leave this issue as unresolved in the present study.

The total radionuclide mass flux versus time exiting the subsite-scale model domain is shown in Figure 6-13. The plateau value for this calculation is an arbitrary value of 145 mol/s for reasons explained above. The time scale of mass arrival at the outskirts of the model are similar to those shown in the concentration breakthrough curves above, but the overall curve is more dispersed. This result is due to the contribution of pathways with lower flow and transport velocities than those leading to points a-d, which were selected to be within the main portion of

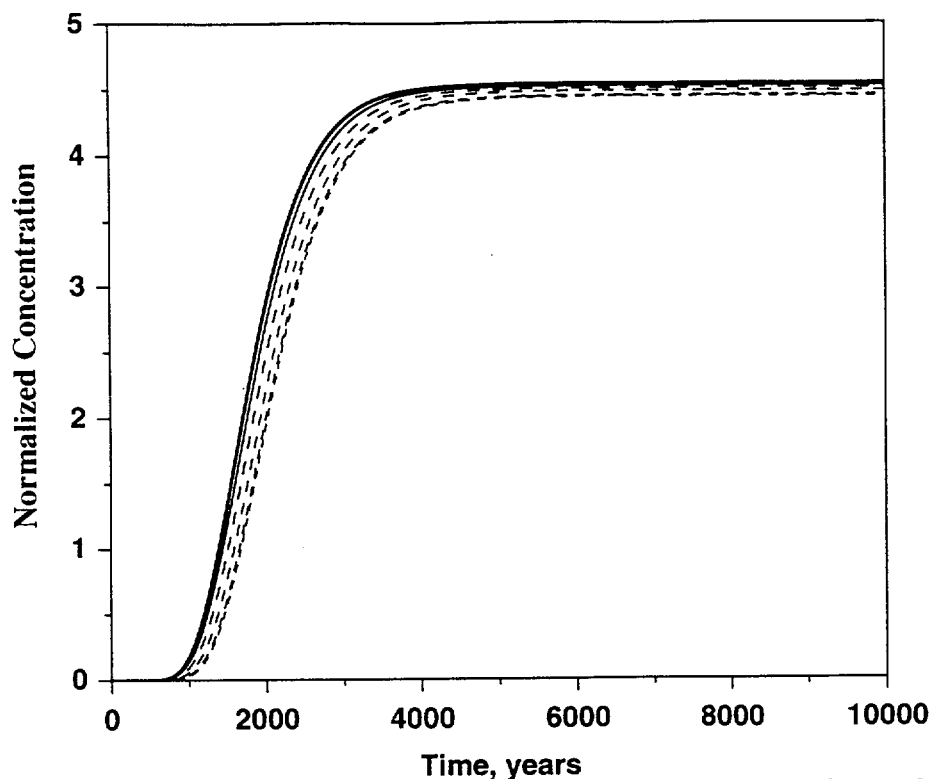


**Figure 6-12.** Concentration time history at four depths at the 5-km center-of-mass location identified as position b in Figure 6-10.

the plume. This curve, or more accurately, the response of this system to an unsaturated-zone mass flux history, can be thought of as the radionuclide *input* to the remainder of the flow and transport system out to more distant compliance points.

In an additional sensitivity study, we examined the influence of sorption onto zeolites on saturated-zone performance. Radionuclides, such as  $^{237}\text{Np}$ , sorb preferentially to zeolitic tuffs, making the identification and distribution of zeolites in the model potentially important for performance. In this study, we map the Project's representation of zeolite distribution (Chipera et al., 1997a) onto the subsite-scale model grid and assign a sorption coefficient of 2 cc/g (Triay et al., 1997) at those locations. Figure 6-14 shows the relationship of the mineralogic model domain and the subsite-scale model in three dimensions, whereas Figure 6-15 is the same comparison from three directions. Clearly, the subsite-scale model is the appropriate one for this procedure, as the

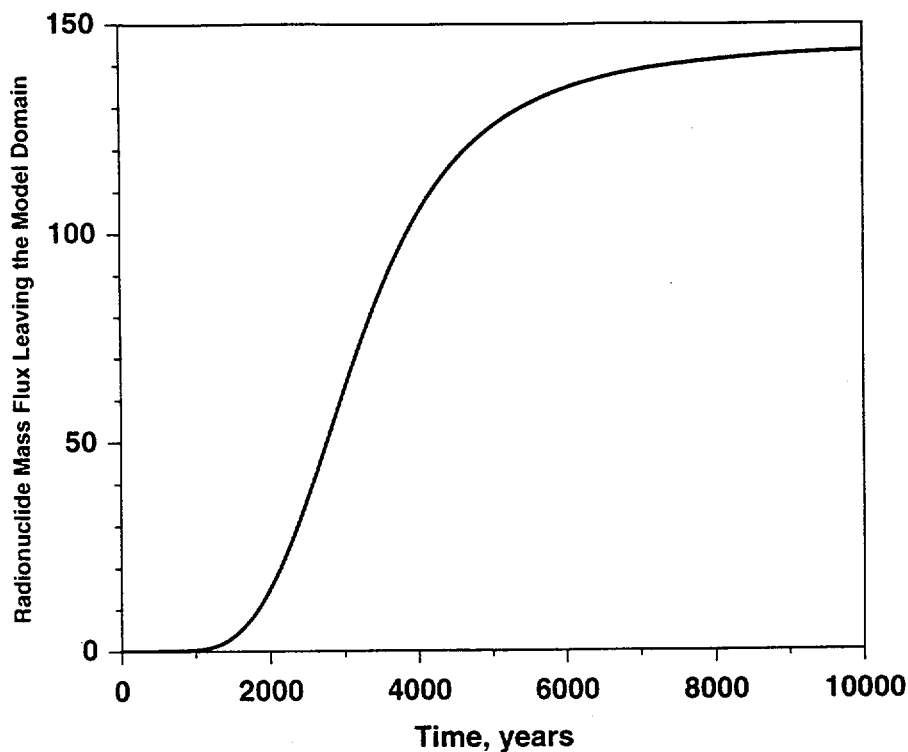
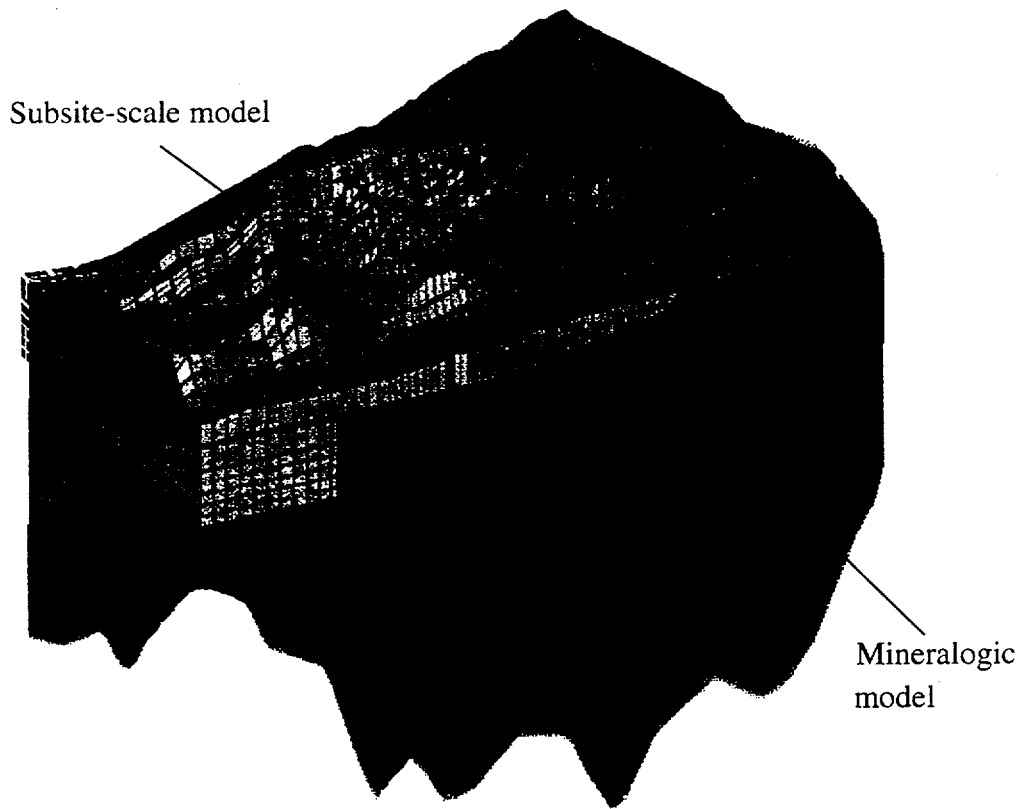


Figure 6-13. Total radionuclide mass flux exiting the subsite-scale model domain.

mineralogic database only extends as far as the outskirts of this model, and no information exists at more distant compliance points such as those studied using the site-scale model. Figure 6-16 compares the generic breakthrough curve at the 5-km center-of-mass location with and without sorption. Sorption has a potentially large impact on the performance of the saturated zone for sorbing radionuclides such as  $^{237}\text{Np}$ . Though sorption coefficients of order 2 cc/g (a typical value for  $^{237}\text{Np}$  sorption onto zeolites, from Triay et al., 1997) are generally considered to imply weak sorption, the predictions show considerable travel time delays. Therefore, sorption of certain radionuclides in the saturated zone will provide a significant barrier to migration.



**Figure 6-14.** Relationship of subsite-scale model domain and the mineralogic model of Chipera et al. (1997a).

## 6.8 Site-Scale Transport Results

---

The continued migration of the radionuclide plume calculated with the subsite-scale model is now predicted using the USGS/Los Alamos site-scale model. A uniform contaminant flux rate is applied to a region representing the interface between the subsite-scale model and the site-scale model as shown in Figure 6-6. This region is downgradient from the repository footprint. Contaminant breakthrough to the southern boundary of the site-scale model, some 30 km from the repository, is calculated using both matrix-like and fracture-like porosity values to show the effect

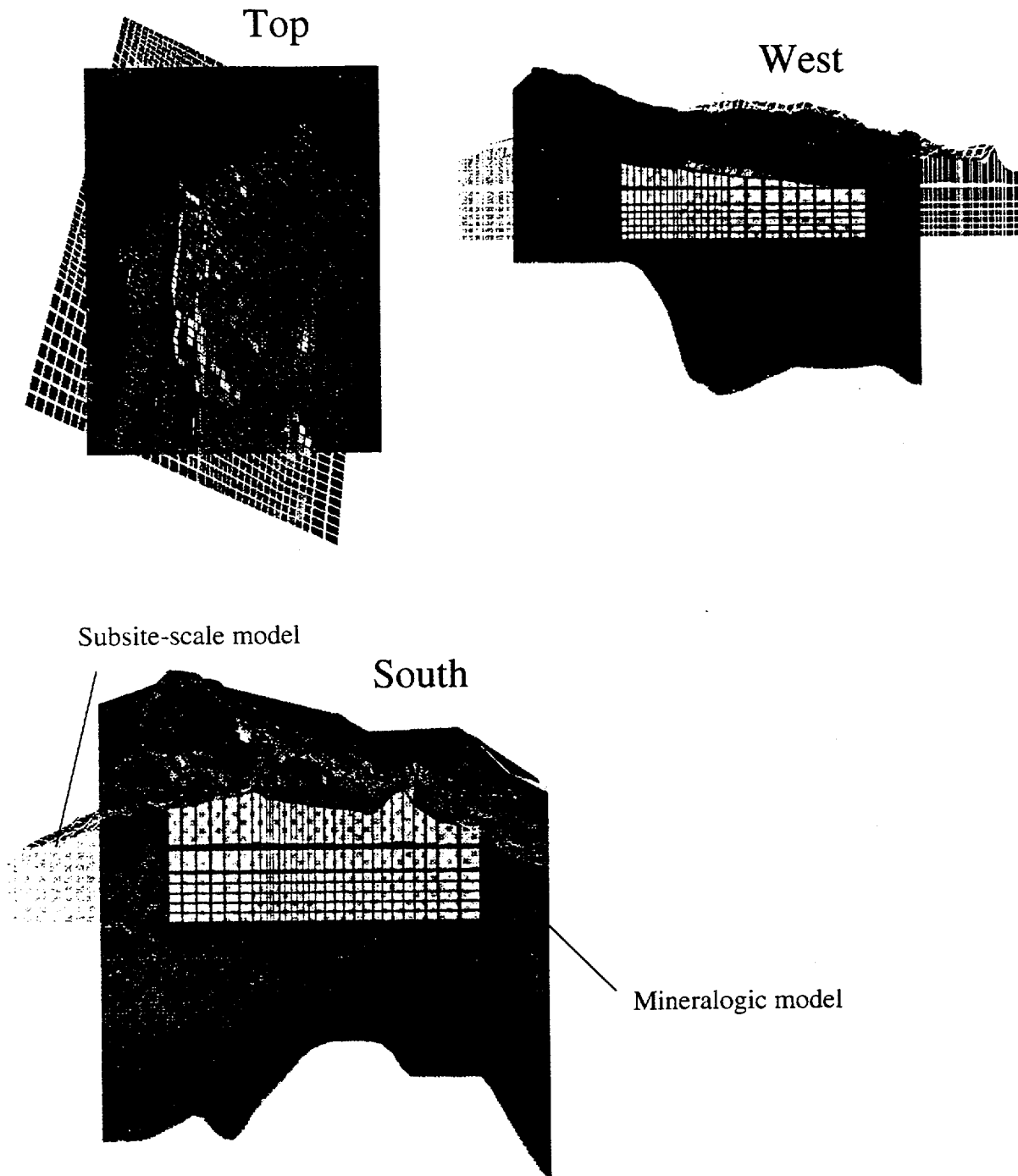


Figure 6-15. Relationship of subsite-scale model domain and the mineralogic model of Chipera et al. (1997a). Top and two side views.

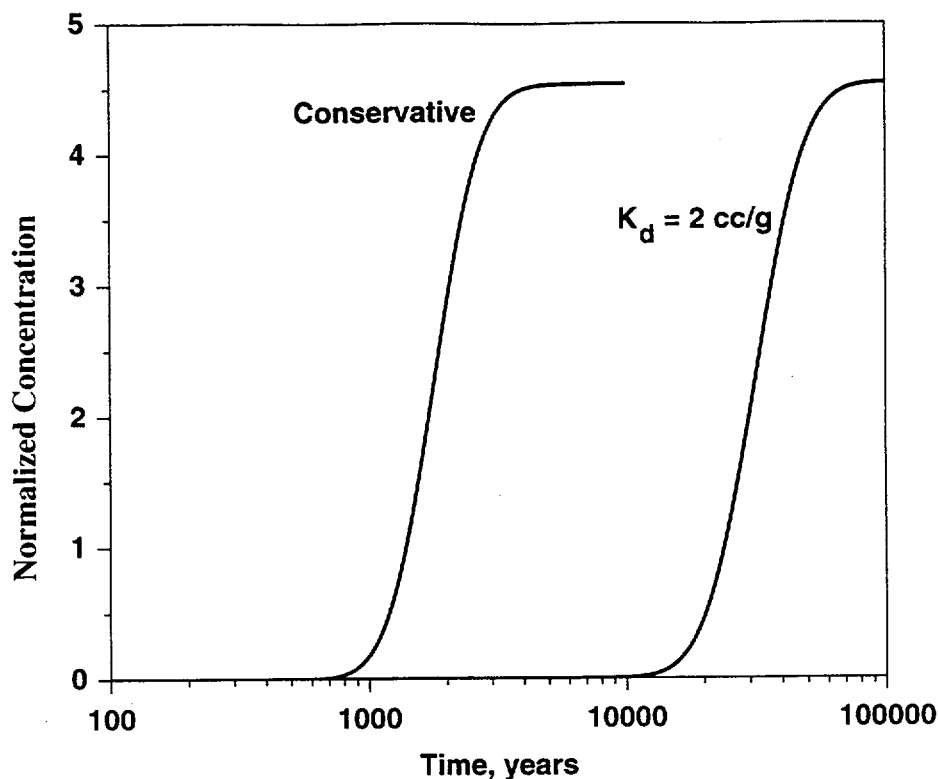


Figure 6-16.  $^{237}\text{Np}$  breakthrough curve at the 5-km center-of-mass location of the site-scale model with and without zeolite sorption.  $K_d = 2 \text{ cc/g}$  for the sorbing case.

of porosity on saturated-zone travel times. Table 6-3 shows the matrix and fracture porosity values used in the simulations. These porosities are based on values from Czarnecki et al. (1997), which are also presented in the table. The matrix porosities used in the simulations are generally taken to be the average between the high and low values given by Czarnecki et al. (1997). The fracture porosities are generally  $10^{-4}$ . The exception is for units having a reported low porosity less than 0.01. In this case, the low value is considered to be the fracture porosity and the high value is considered to be the matrix porosity for that particular unit. The alluvial, valley-fill aquifer (unit 19) is considered to be a porous continuum with large porosity; for this unit the average matrix

**Table 6-3. Matrix and Fracture Porosities used in Site-Scale Simulations**

Hydrogeologic Unit (unit number)	Values Reported by Czarnecki et al. (1997)		Values Used in Simulations	
	High	Low	Matrix	Fracture
Valley-Fill Aquifer (19)	0.23	0.12	0.175	0.175
Valley-Fill Confining (18)	0.66	0.29	0.475	1.e-4
Lava-Flow Aquifer (16)	0.11	0.004	0.11	0.004
Upper Volcanic Aquifer (15)	0.544	0.014	0.279	1.e-4
Upper Volcanic Confining Unit (14)	0.503	0.123	0.313	1.e-4
Middle Volcanic Aquifer (13)	0.436	0.018	0.227	1.e-4
Middle Volcanic Confining Unit (12)	0.274	0.092	0.183	1.e-4
Lower Volcanic Aquifer (11)	0.384	0.081	0.232	1.e-4
Lower Volcanic Confining Unit (10)	0.17	0.088	0.129	1.e-4
Lower Valley-Fill Confining Unit (9)	0.30	0.10	0.20	1.e-4
Tertiary Limestone Aquifer (17)	no data	no data	0.30	1.e-4
Granitic Confining Unit (2)	0.07	4.e-5	0.07	4.e-5
Upper Carbonate Aquifer (8)	0.16	0.005	0.16	0.005
Upper Clastic Confining Unit (6)	0.151	0.006	0.151	0.006
Lower Carbonate Aquifer (3,5,7)	0.16	0	0.16	1.e-4
Lower Clastic Confining Unit (4)	0.07	4.e-5	0.07	4.e-5

value is used for both simulations. Figure 6-17 shows concentration breakthrough curves at the southern boundary of the site-scale model. These curves are based on a constant flux rate of 1 mol/s applied to 13 nodes that represent the interface between the subsite-scale and site-scale models (for a total of 13 mol/s). As discussed in Section 6.5, the concentration scales are arbitrary but allow for a comparison between the matrix- and fracture-porosity travel times. The travel times are quite long. For the fractured media, the midpoint of the breakthrough curve arrives after about 10 ky, and for the matrix media, it is about 37 ky. When the alluvium is considered to be slightly

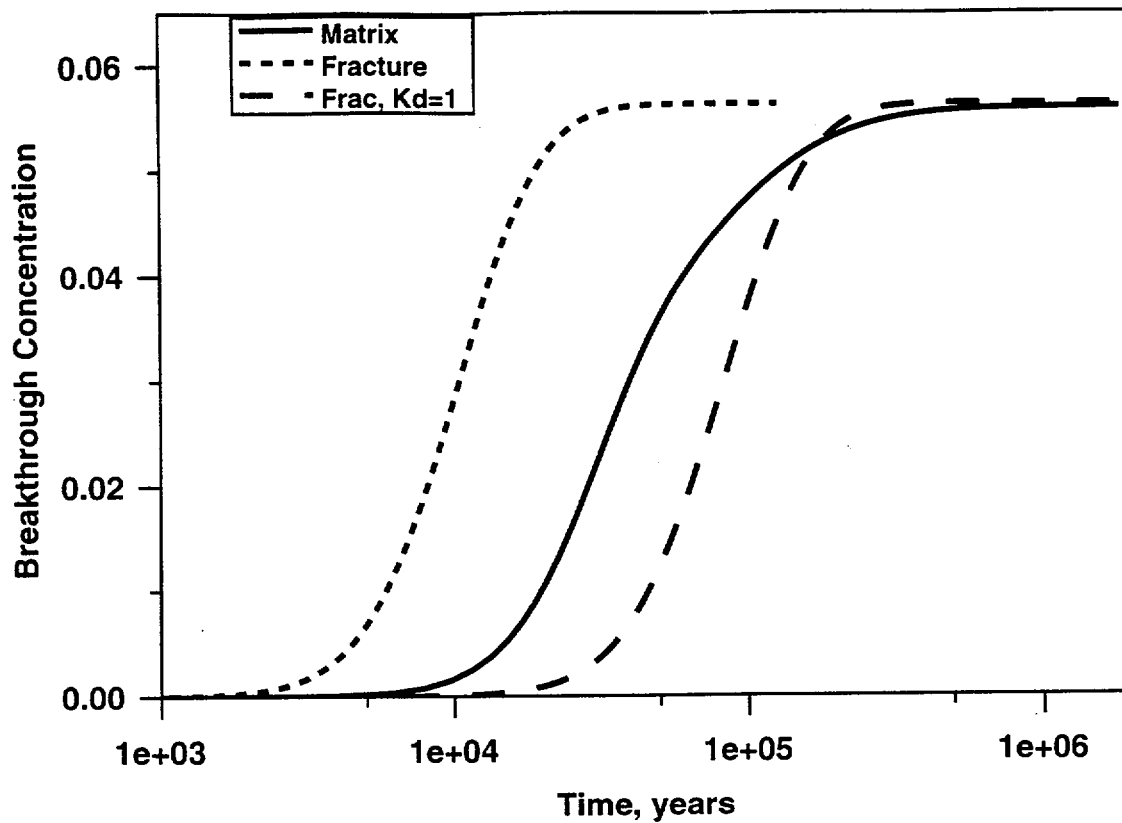


Figure 6-17. Breakthrough curves at the southern boundary of the site-scale model using matrix porosity, fracture porosity, and fracture porosity with sorption ( $K_d = 1$  cc/g) in the alluvium.

sorbing ( $K_d = 1$  cc/g), the predicted mean travel time grows to about 80 ky, even for the case in which the tuff aquifer is assumed to have a low effective transport porosity. Figure 6-18 shows a contour plot of the steady-state plume.

In the breakthrough predictions shown in Figure 6-17, most of the travel time is due to porous flow and transport in the alluvium. In these simulations, a minimum travel time of several thousand years is predicted due to porous flow and transport in the alluvium. We note this because the extension of compliance distances to 20 km or more has brought into play units other than fractured volcanic tuffs, and system performance is likely to be controlled by a part of the hydrologic system that has received little attention. Finally, we should note that, because these simulations were run with the coarse 1500-m grid spacing, the results are dispersive and, therefore,



**Figure 6-18.** Concentration profile of plume in the site-scale model. North is at the top of the figure. nonconservative. However, the results illustrate the system behavior and yield a good approximation of saturated-zone travel times.

### 6.9 Validation of the Numerical Convolution Technique

---

In Section 6.3, we outlined a convolution method to compute the concentration time response of an actual radionuclide at a compliance point. A generic breakthrough curve, such as one of the results in Figure 6-11, is used as the kernel in a convolution calculation with the input being the mass flux at the water table predicted from an unsaturated-zone transport calculation. We now demonstrate the use of this approach and prove the validity of the numerical implementation, comparing it to a full calculation of radionuclide transport in the model with the mass flux versus time input directly to the footprint. For this simulation, we take the results of a typical two-dimensional unsaturated-zone simulation of  $^{99}\text{Tc}$  (in Robinson et al., 1997: Case 6541, base infiltration map, 3 ky constant duration release) shown as the dotted curve in Figure 6-19. Also

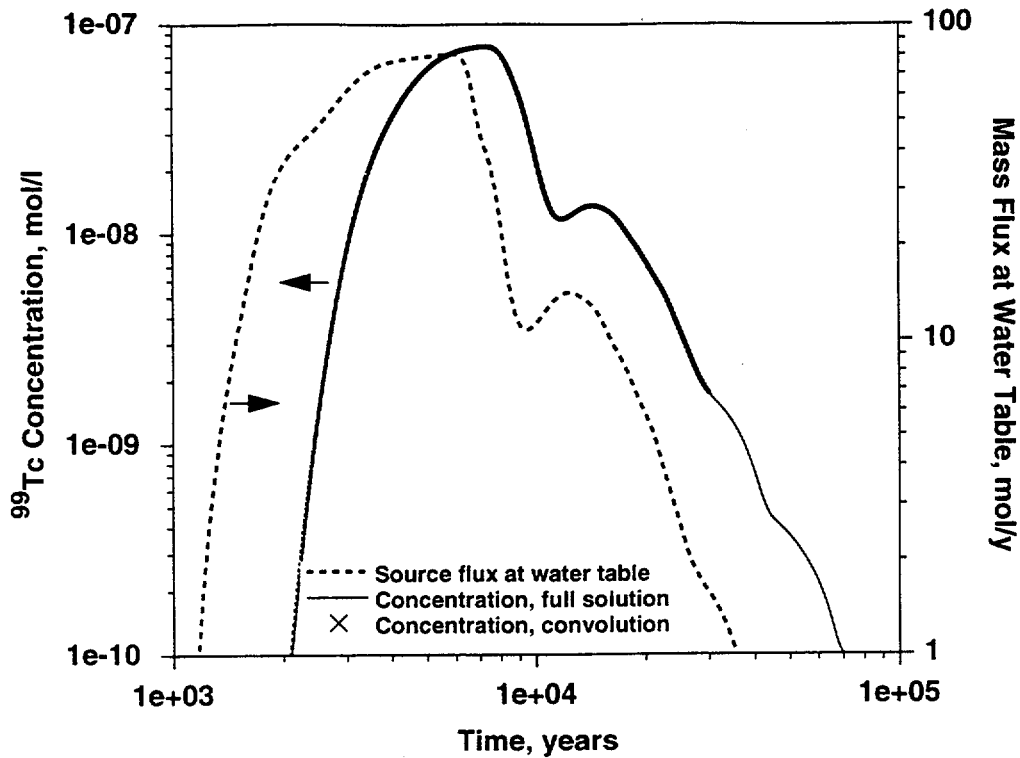


**Figure 6-19.** Predicted breakthrough curves at the 5-km center-of-mass location of the subsite-scale model. Dotted curve: mass flux input at the water table (curve refers to the right y-axis). Solid curves: breakthrough curves computed directly (solid curve) and by convolution (red x's).

shown are the simulation results for two cases. The curve labelled "convolution" uses the generic breakthrough curve for the 5-km center-of-mass location at the water-table elevation from Figure 6-11 as the kernel, and the dotted curve is the input function. The "full solution" curve is a direct numerical simulation result using the saturated-zone model itself for the calculation, with mass flux input into the water-table nodes read from a table built from the results from the unsaturated-zone calculation. The differences are imperceptible, illustrating that the convolution method has been accurately implemented. The benefit of the method is computational efficiency. First, the saturated-zone calculation only needs to be carried out until the concentration at the compliance point reaches its plateau. Typically, the overall prediction needs to be carried out to much longer times (up to one million years); significantly, the saturated-zone calculation itself is not tied to this simulation time if convolution is used. Furthermore, with convolution, only one saturated-zone calculation needs to be computed for each saturated-zone realization, and any near field/

unsaturated-zone realization can be easily coupled to this saturated-zone model without recomputing the saturated-zone radionuclide migration.

There are other issues related to the validity of the convolution method that go beyond verification of correct numerical implementation. These include:

- the steady-state assumption for fluid flow;
- linearity of transport processes; and
- spatial variability of radionuclide mass flux input from the unsaturated zone.

To be addressed in a comprehensive way, the first issue must be investigated with a site-scale or regional-scale flow and transport model in which the recharge is an input boundary condition. In this way, the fluid source can be increased by a set amount to simulate the influence of a wetter future climate. Because this model is not available at present, we perform an approximate analysis to estimate the potential for climate-induced changes to the flow and transport system. This study is carried out in Section 6.11.

Regarding the linearity of radionuclide migration processes, transport in the absence of chemical effects is linear, and the only sorption model used in the saturated-zone modeling is the linear- $K_d$  model. This simplification requires that the sorption coefficient be estimated at the anticipated conditions of the transporting plume. Typically, nonlinear sorption is parameterized using a concentration-dependent sorption isotherm. These isotherms have been measured for a few radionuclides, most notably  $^{237}\text{Np}$  and uranium by Triay et al. (1996b, c). For  $^{237}\text{Np}$ , concentration dependence of the sorption  $K_d$  is small to nonexistent. For uranium, Triay et al. (1996b) determined values of  $K_d$  on zeolitic tuffs ranging from 5 cc/g at  $10^{-4}$  mol/l to 20 cc/g at  $8 \times 10^{-8}$  mol/l. The solubility of uranium is approximately  $10^{-4}$  mol/l, so by the time fluid with this concentration is diluted in the saturated zone, concentrations at the low end of the range of measured  $K_d$  values are expected. Therefore, the larger  $K_d$  values should be used for uranium, and nonlinearities brought on by concentration dependence can be ignored. If other data are collected

suggesting concentration-dependent sorption, the linear- $K_d$  model can be used conservatively by assuming the  $K_d$  value at the highest expected concentration values. In this way, the linear assumption underlying the convolution assumption can be retained.

Another transport process that would violate the linearity assumption is precipitation of radionuclides. It has been suggested (Meijer, in Triay et al., 1996a) that the redox conditions of the saturated zone may be more reducing with depth. The implications for transport of key radionuclides such as  $^{99}\text{Tc}$  and  $^{237}\text{Np}$  are dramatic. Under somewhat more reducing conditions than the saturated-zone fluid near the water-table surface, these two mobile radionuclides would be reduced to lower oxidation states with dramatically reduced solubilities and increased sorption coefficients. Increased sorption can be handled with an increased sorption coefficient with depth without violating the linear assumption. Precipitation cannot be included in a linear transport model, however. If site data to be collected in the next year indicate that precipitation deeper in the saturated zone is likely, we will have to revisit the linear assumption. However, until then, we assume that oxidizing conditions exist throughout the saturated zone along likely radionuclide migration pathways. From the arguments above, it therefore follows that there are no confirmed nonlinear chemical processes that violate the linear assumption of the convolution method.

The final issue related to the convolution method, spatial variability in radionuclide mass flux at the water table, is really an issue of how the convolution method is implemented rather than whether it is valid. Spatial variability, if important, means that individual breakthrough curves would need to be generated for different regions on the repository footprint. Then the concentration time response at a given location could be obtained by superposition of the individual convolution calculations. Obviously, simplifications to an involved procedure like this would be desirable, but spatial variabilities of the input to the saturated zone do not, in themselves, violate the assumptions of the convolution process. In the next section, we examine the possibility of spatial variability in greater detail.

### 6.10 Spatial Variability in Radionuclide Flux

---

The details of radionuclide migration in the unsaturated zone are controlled by flow and transport processes such as fracture and fault controls and infiltration rate spatial variability. For our purposes, these processes may give rise to source-term variability in space and time. Spatial variability would be present if, for example, transport pathways in the unsaturated zone all channeled to a fault that feeds radionuclides to the water table in one location or along the trace of the fault at the water table. Temporal variability, though not as obvious, could also play a role. The percolation flux at the repository horizon is expected to be highly variable with portions of the repository possibly releasing radionuclides early in the time frame of a performance calculation and with slower releases in another portion of the repository. This variability could be reflected in a different source term for different locations in the footprint. Thus, it is important to examine the implications of any differences in downstream breakthrough curves caused by the position of release at the water table.

Given that the primary control on saturated-zone transport behavior is likely to be stratigraphic units with contrasting permeabilities, we divided the nodes comprising the repository footprint into subsections based on stratigraphy. Specifically, individual transport calculations were performed for the footprint nodes that fall within the Prow Pass, Bullfrog, and Tram units. The plumes for each of these transport simulations are shown in Figures 6-20, 6-21, and 6-22. The solute plume at the water table for the Prow Pass and Bullfrog units are similar to one another and are responsible for the portion of the overall plume with the southeasterly migration direction. The Bullfrog plume tends to migrate somewhat more south than does the Prow Pass plume, but the results are quite similar. By contrast, the Tram plume travels almost due south. Relating these plumes to the location beneath the repository, the Tram plume shows the likely direction of radionuclides issuing from the southern end of the repository because this is the only location where the first unit encountered below the water table is the Tram. Regarding the similarity of the Bullfrog and Prow Pass plumes, each travel in the direction of the presumed pressure gradients

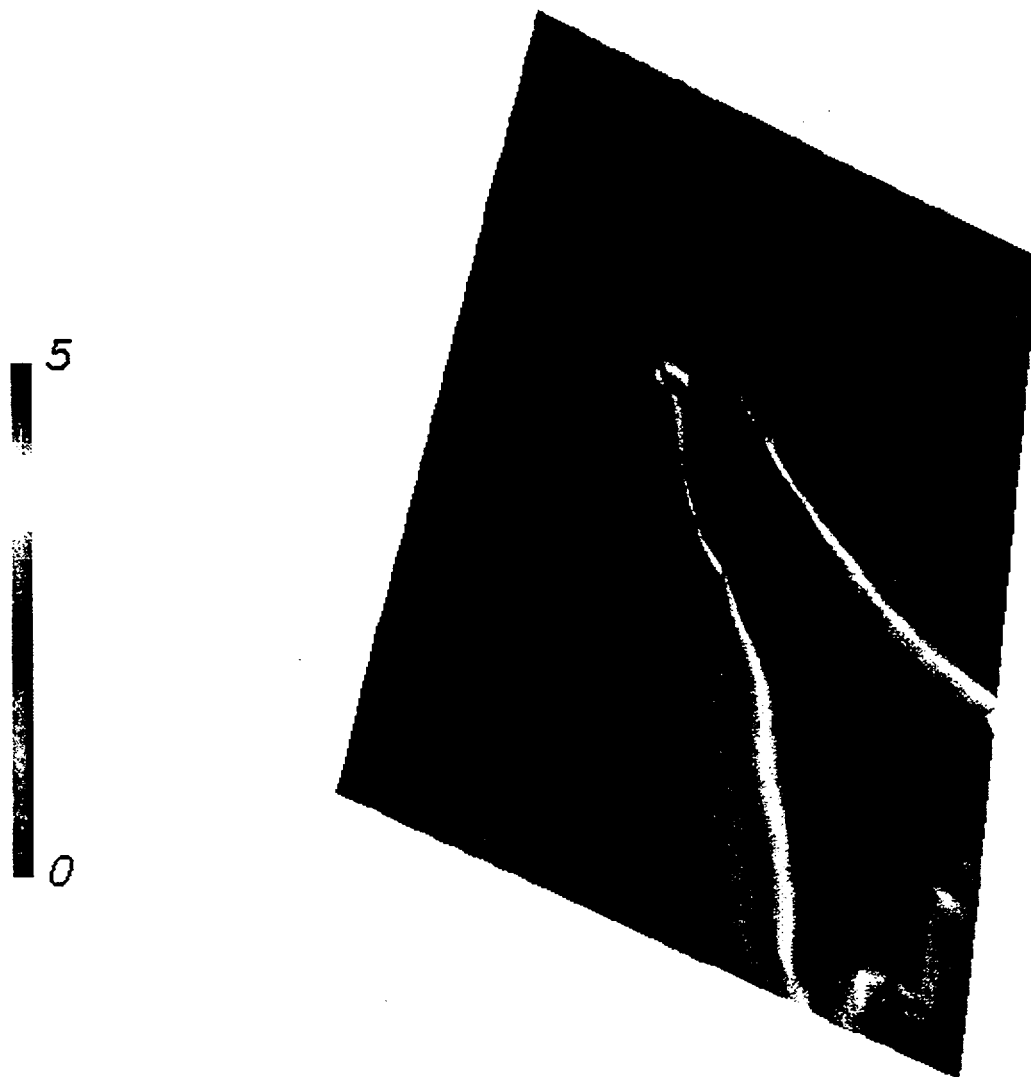


**Figure 6-20.** Predicted plume for radionuclides released at the water table into the Prow Pass unit. North is at the top of the figure.

(locally to the east and south) within the permeable units in that direction. This effect occurs primarily in the Prow Pass tuffs out to the boundary of the model. In fact, radionuclides that enter the saturated zone in the less permeable Bullfrog unit probably travel to the Prow Pass unit and travel in the same pathways as radionuclides that enter the saturated zone in the Prow Pass. Therefore, the main distinction with respect to the origin of the radionuclides at the water table appears to be whether radionuclides enter the Tram unit or the Prow Pass or Bullfrog units.

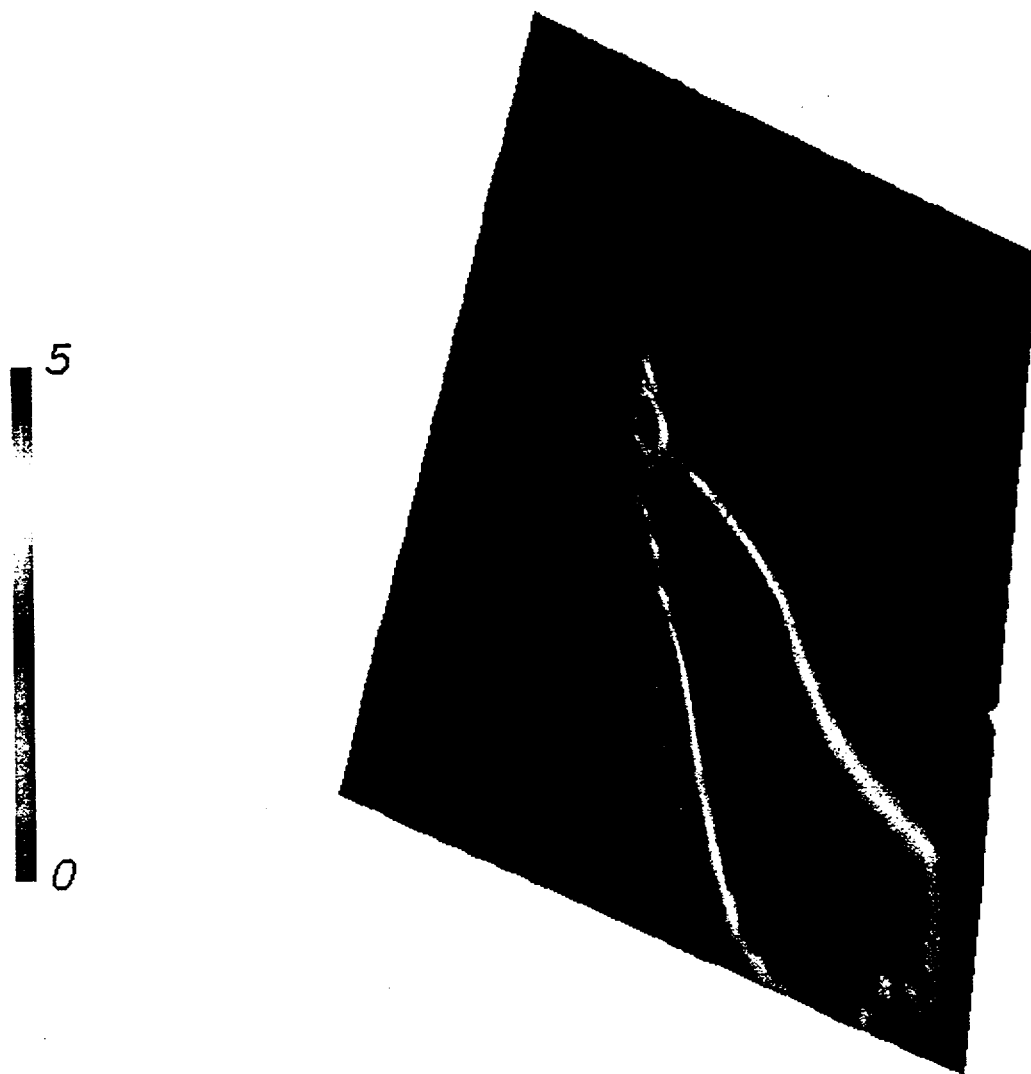


**Figure 6-21.** Predicted plume for radionuclides released at the water table into the Bullfrog unit. North is at the top of the figure.

The previous discussion presumes that radionuclides travel vertically downward from the repository to the water table. The concept of a repository footprint as the source locations of radionuclides in the saturated zone is only valid when this assumption is true. An alternative concept that needs to be considered is one of lateral flow to major fault zones that act as drains of the unsaturated-zone system. Such a fault would be the primary pathway for radionuclides under that type of scenario. The most likely fault that could provide such a pathway is the Ghost Dance fault, due to its location down-dip from the repository. This fault intersects the water table in the

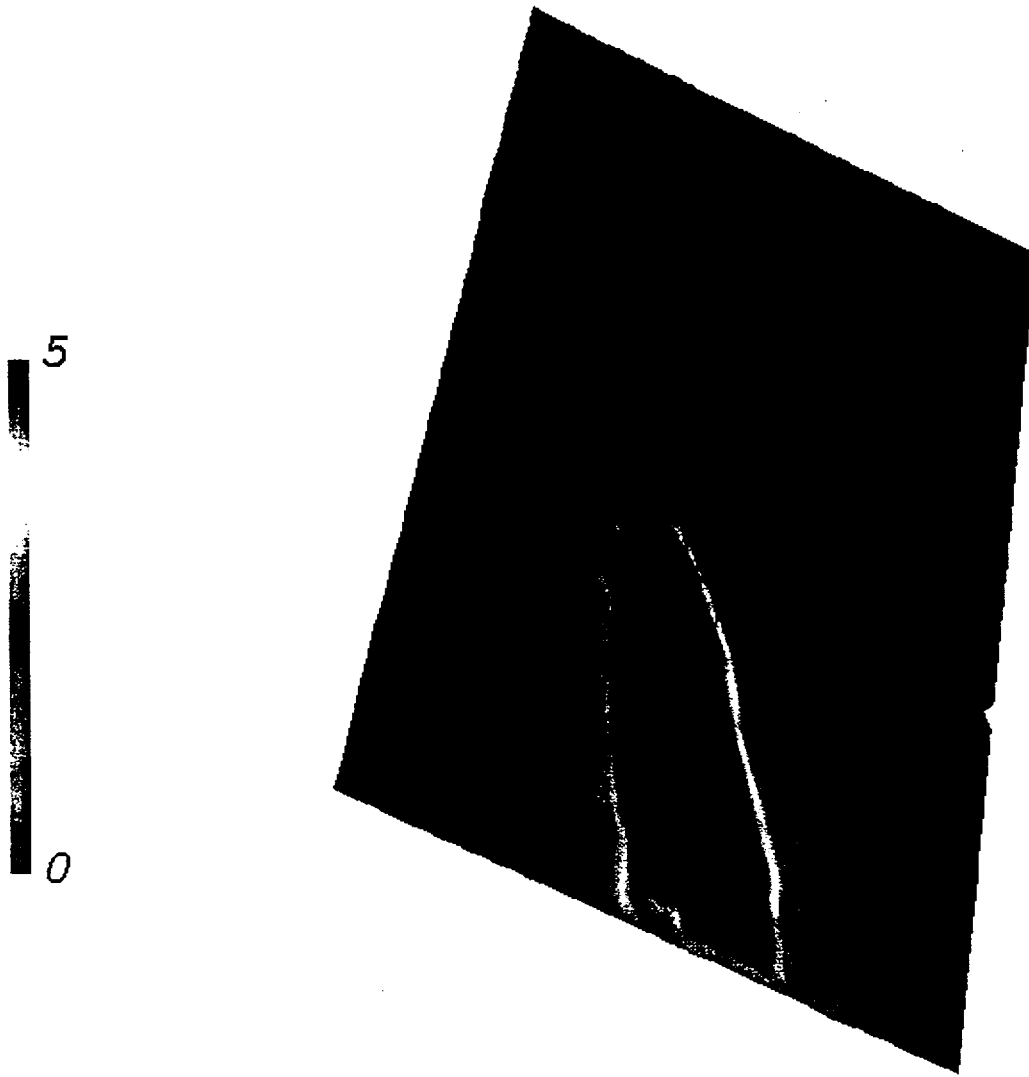


**Figure 6-22.** Predicted plume for radionuclides released at the water table into the Tram unit. North is at the top of the figure.

Prow Pass formation, so that the predicted pathways of radionuclides would be those of Figure 6-20. On the other hand, if laterally diverted flow at the TSw basal vitrophyre or within the Calico Hills unit is able to traverse the Ghost Dance fault, radionuclides would likely reach the water table in the Calico Hills unit in locations similar to those investigated by Altman et al. (1996) in their study of the original, larger repository area. Because of the presence of the Ghost Dance fault, we consider this scenario less likely but point it out because of the implications for performance. As

mentioned earlier, Altman et al. (1996) computed longer travel times for particles initiated in the Calico Hills unit because of its lower permeability.

Another way to examine spatial effects is to compute individual breakthrough curves from different repository footprint locations at a given downstream location. Figure 6-23 shows such a

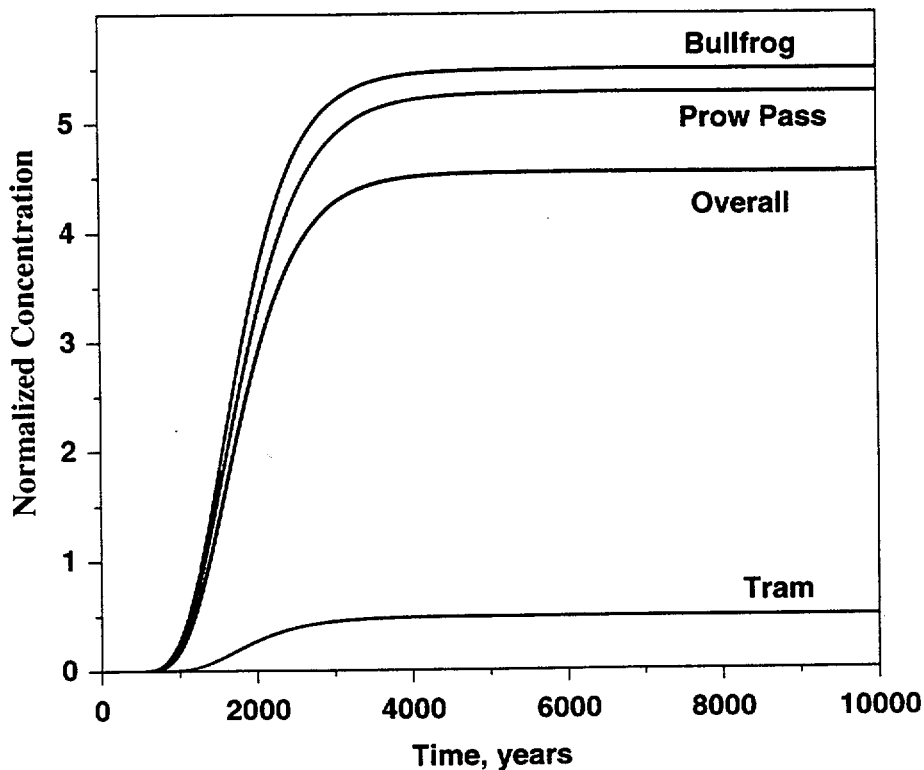


**Figure 6-23.** Breakthrough curves at location b for radionuclide mass released at the water table at each of the three individual units.

plot for the three subsections of the repository footprint for breakthrough at the 5-km center-of-mass location. For each simulation, the same input mass flux was assumed. Therefore, plateau concentrations greater than the overall breakthrough curve indicate the source region supplying radionuclide at the 5-km center-of-mass location is weighted more heavily toward that inlet region. At this location, radionuclide from the Prow Pass and Bullfrog subregions of the footprint supply most of the radionuclides that pass through at this location, whereas radionuclide entering in the Tram misses this position. As shown earlier, this radionuclide travels almost due south and, thus, does not contribute significantly to the breakthrough at positions b, c, or d of Figure 6-10.

Despite these differences within the first 5 km along the saturated-zone radionuclide pathways, transport at greater distances is likely to be less sensitive to these details. Figure 6-24 plots the mass-flux curve for all radionuclide leaving the subsite-scale model domain for radionuclide entering uniformly across the footprint and for individual subregions. Such a plot is, in essence, a radionuclide source term for the remaining transport paths to a more distant accessible environment boundary. The curves are very similar, suggesting that for distances exceeding 5 km, details of radionuclide pathways near the site are relatively unimportant.

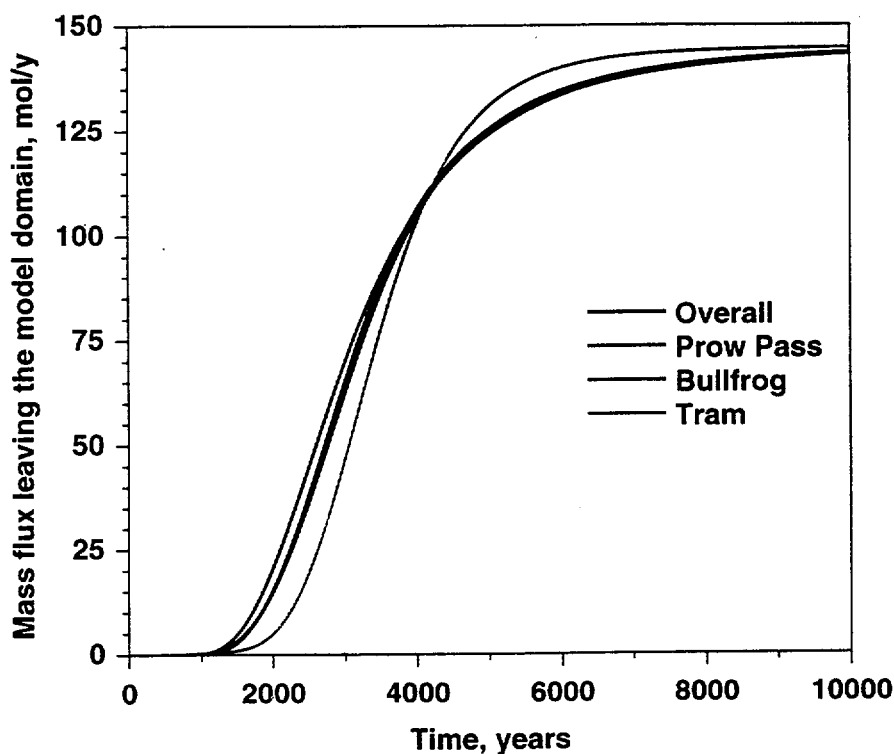


**Figure 6-24.** Overall mass flux exiting the model domain for individual injection of radionuclides in each of the injection zones.

### 6.11 Uncertainty in Flow and Transport Parameters

From the results presented so far, we have identified several parameters and processes that exert important controls on the overall behavior of the saturated-zone flow and transport system. These include dispersion, fluid flux, and the extent of matrix diffusion. In this section, we examine the impact of key uncertainties in the saturated-zone model on transport of radionuclides. Because

the grids used in the site-scale and subsite-scale flow and transport modeling do not at present have sufficient resolution to minimize numerical dispersion artifacts, we focus on fluid flux and matrix diffusion in this section. Dispersion was treated earlier in the highly resolved but idealized flow and transport calculations presented in Section 6.4.

### 6.11.1 Uncertainty in Fluid Flux

We first examine the influence of permeability and its impact on flow velocities and transport. Fluid flux beneath the repository could be different than predicted here for two reasons. First, because the calibrated models of the present study use only head boundary conditions, the fluid velocities in the model are not well constrained. Although the comparison to flux values derived from the regional-scale model are encouraging, there is still considerable uncertainty. By adjusting the permeability of each unit up or down by a constant factor, the pressure field in the system remains the same (the model is calibrated to the same precision as for the original case), but the flow velocities are directly proportional to the permeability. Second, a future, wetter climate would likely give rise to higher fluxes within the saturated zone.

To test the influence of saturated-zone fluid flux on performance, all permeabilities in the subsite-scale model were adjusted upward by a factor of five. Although the simulation is posed as uncertainty in permeability values, it can also be viewed as a proxy for a future, wetter climate scenario in which the flux underneath Yucca Mountain increases. First, we compared the pressure distributions for the two cases and found that they agreed to within 0.01 MPa at all locations. The concentration versus time at the 5-km center-of-mass location was affected dramatically, however. Figure 6-25 compares the generic breakthrough curves, and Figure 6-26 shows the result obtained by numerical convolution for the  $^{99}\text{Tc}$  case considered in the previous section on the convolution technique. Transport times to a given location are shortened for the high-permeability, high-flux case, but the plateau concentration in the generic breakthrough curve (Figure 6-25) is reduced due to increased dilution at the higher fluid flux. The result is a radionuclide breakthrough (Figure 6-26) that occurs somewhat sooner, but the peak concentration is lower.

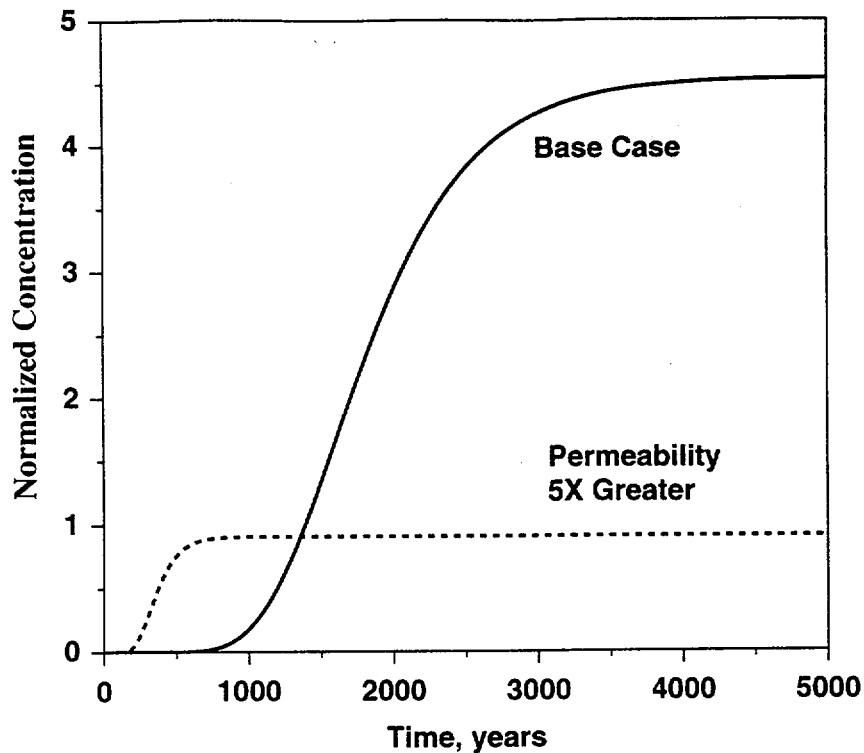


**Figure 6-25.** Comparison of breakthrough curves at the 5-km center-of-mass location of the sub-site-scale model for the base case and a case with five times greater permeability at all locations.

Although statements on the relative importance of travel time versus concentration value are difficult to make without a definitive set of regulatory criteria, it seems likely that the dilution benefit of a greater saturated-zone flow velocity will outweigh the more rapid travel times that occur as a result. Peak dose values will be directly linked to concentration, so lower predicted concentrations imply lower doses. The uncertainty in interpreting these results lies in the regulatory time frame and compliance distance selected for the site. If the combined “delay times” of the engineered, unsaturated-zone, and saturated-zone transport barriers exceed the regulatory time frame in which doses are relevant, then the dose will be zero. Rapid transport through the saturated zone would only become a detriment to performance if it displaces the overall breakthrough curve to times less than the compliance period. Regarding the distance to the accessible environment boundary, let us take a 5-km boundary as an example. Because, for current performance predictions, conservative radionuclides are predicted to reach a 5-km accessible

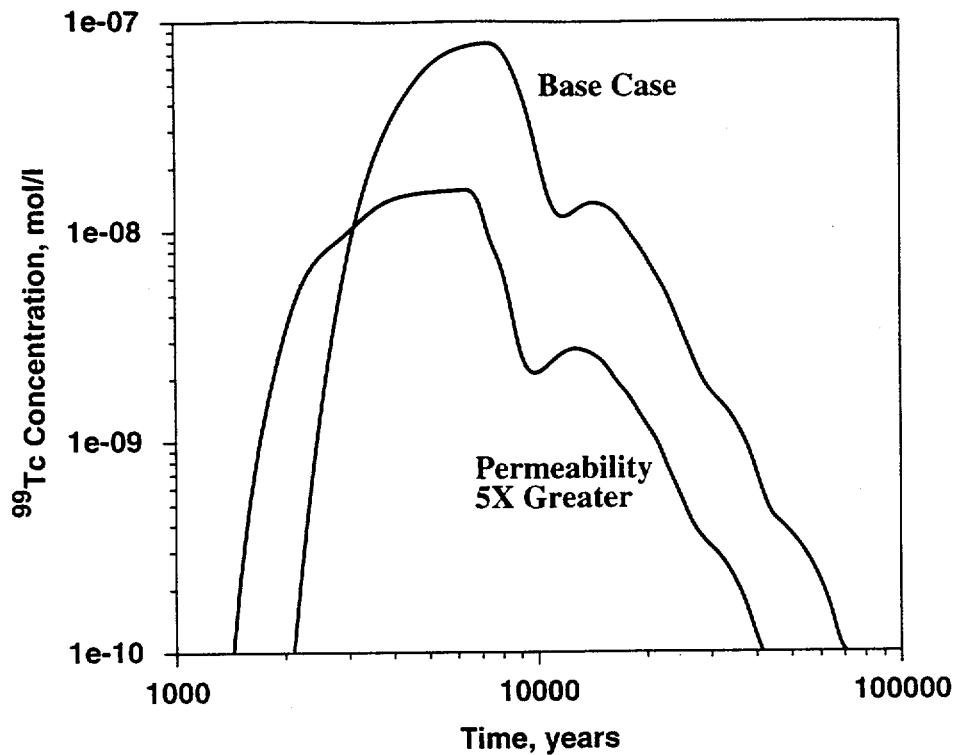


**Figure 6-26.** Comparison of  $^{99}\text{Tc}$  breakthrough curves at the 5-km center-of-mass location of the subsite-scale model for the base case and a case with five times greater permeability at all locations. Water-table source term shown in Figure 6-19.

environment in less than 10 ky, the exact travel time is unimportant, and the increased dilution resulting from higher fluxes is beneficial to performance. If the accessible environment boundary is 20 km, however, travel times in the saturated zone may be large enough to push the radionuclide breakthrough curve to greater than 10 ky. By contrast, if the compliance period is 100 ky, the travel time will be unimportant and the dilution effect of higher flow velocities will be the factor influencing the dose.

Regardless of the circumstances, the performance of the site is clearly tied to the fluid flux in the saturated zone, so methods to estimate flow velocities more precisely under current and anticipated future conditions are critical. For present-day conditions, calibration to measured heads is not enough; independent estimates of flux are required to constrain model predictions. This application of flux information is not easily done at either the subsite or site scale. The regional-scale model provides the areal extent needed to capture the actual recharge and discharge

fluxes that make up the inlet and outlet flows for the groundwater flow system. At smaller scales, the flow rates into and out of model faces are not really measurable or traceable to measured flux values. Alternatively, fluxes across a site-scale model boundary can be obtained from the regional-scale model and used as input in the smaller-scale model. This method has its own set of difficulties, including different geologic framework model descriptions in the region of overlap and the lack of detail in the larger-scale model, which was not intended to capture detailed flow patterns and processes near Yucca Mountain. In the present study, we instead compared the flux values from the regional- and site-scale models and found them to be consistent (see Section 3.4). Regarding the subsite-scale model, additional difficulties arise because of the greater depth of the site-scale model, making direct comparisons problematic. We anticipate that when the ISM 2.0 geologic framework model (Clayton et al., 1997) shown in Figure 3-4 is built into the site-scale flow and transport model, many of these problems will be mitigated. Until then, we regard the flux through the model domain in the vicinity of Yucca Mountain as one of the key uncertainties in the model.

### 6.11.2 Uncertainties in Matrix Diffusion Parameters

In Section 5.6, we outlined the concept of matrix diffusion and its potential for increasing radionuclide travel times in the saturated zone. In this section, we apply these concepts to transport in the subsite-scale model. To vary the extent of matrix diffusion in the model, we use the approximate method developed in Section 5.6 and illustrated in Figure 5-3 in which the effective porosity for transport is the parameter that modulates the influence of matrix diffusion on breakthrough. Figure 6-27 illustrates the impact on the generic saturated-zone breakthrough curves, and Figure 6-28 shows how this uncertainty influences the concentration of  $^{99}\text{Tc}$  at the 5-km accessible environment boundary (the 5-km center-of-mass location, position b). The generic breakthrough curves exhibit a large difference in arrival times, but because the fluid flow rate through the medium is presumed to be constant for each case, the plateau concentration is the same for each. This effect results in a  $^{99}\text{Tc}$  breakthrough curve that differs only in the arrival time

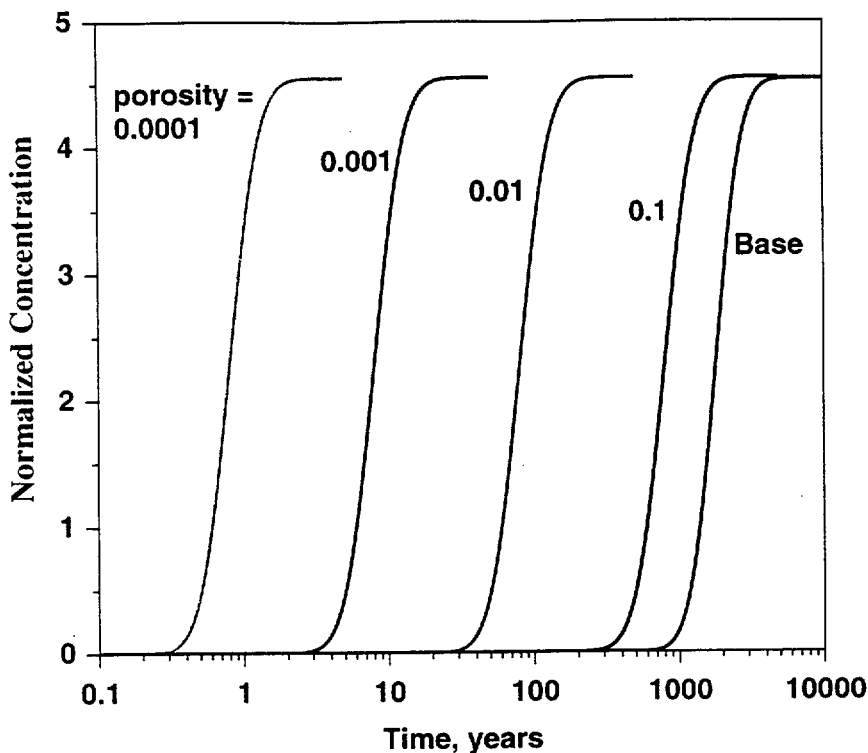


**Figure 6-27.** Comparison of breakthrough curves at the 5-km center-of-mass location of the sub-site-scale model for different values of effective transport porosity.

at the compliance point, but not in the peak value. Thus, the influence is qualitatively different than the case of flow velocity variability, which changed the dilution factor as well as the arrival time.

## 6.12 Influence of Repository Heat

Although repository heat effects are usually thought to exert a more important control on near-field and unsaturated-zone conditions and behavior, heat emitted from the potential repository eventually reaches the saturated zone, where it heats the rock and fluid passing beneath Yucca Mountain. This effect changes the conditions for transport somewhat and, thus, must be examined. These effects are likely to be most pronounced near the repository footprint; conditions are likely to become closer and closer to ambient as one moves away from the site. Thus, in the present study, we use the subsite-scale model to investigate repository heat effects because of its greater

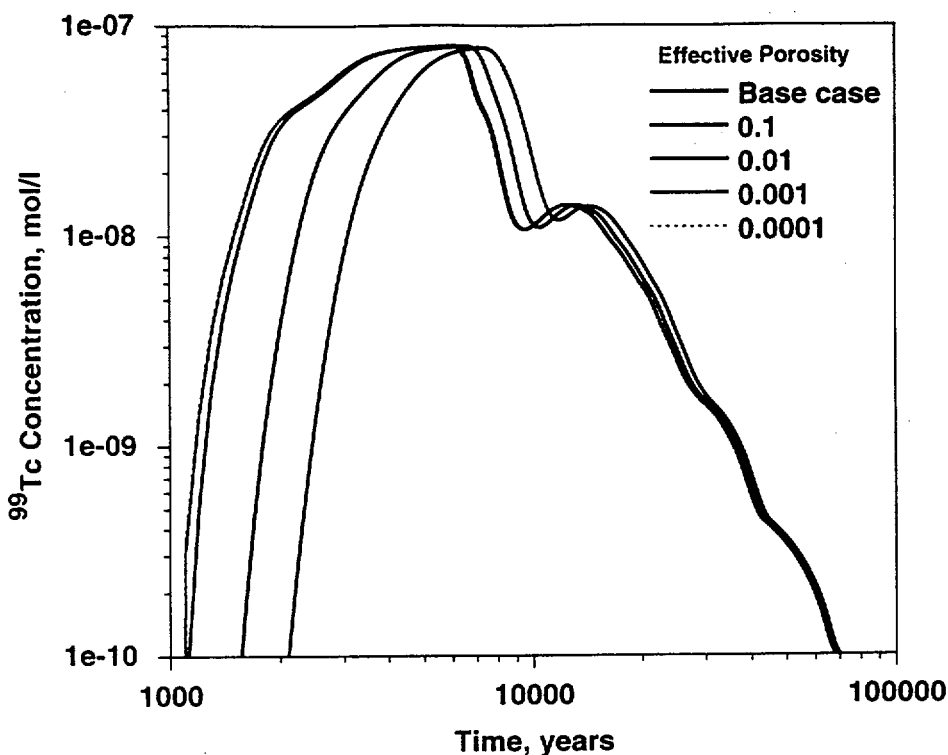


**Figure 6-28.** Comparison of  $^{99}\text{Tc}$  breakthrough curves at the 5-km center-of-mass location of the subsite-scale model for different values of the effective transport porosity. Water-table source term shown in Figure 6-19.

resolution near the site. To simulate approximately the thermal perturbation in the saturated zone, we draw upon the repository heat calculations presented in Robinson et al. (1997). In those calculations, we simulated heat transport in the unsaturated zone and, in addition to performing unsaturated-zone transport simulations, recorded the temperature versus time at a location below the potential repository at the water table. An appropriate abstraction of that result is to assume that starting 1000 years after waste emplacement, the temperature at the water table rises to roughly  $55^{\circ}\text{C}$  and remains elevated for about 30 ky. In this study, we apply this temperature at the repository footprint and compute the transport of fluid, heat, and radionuclides to the compliance points. By comparing the results with the isothermal simulations, we can assess the influence of waste heat on saturated-zone transport.

Figure 6-29 shows the simulated temperature within the model after 30 ky of heating at the repository footprint. The top figure is a horizontal slice at the water table, showing the migration

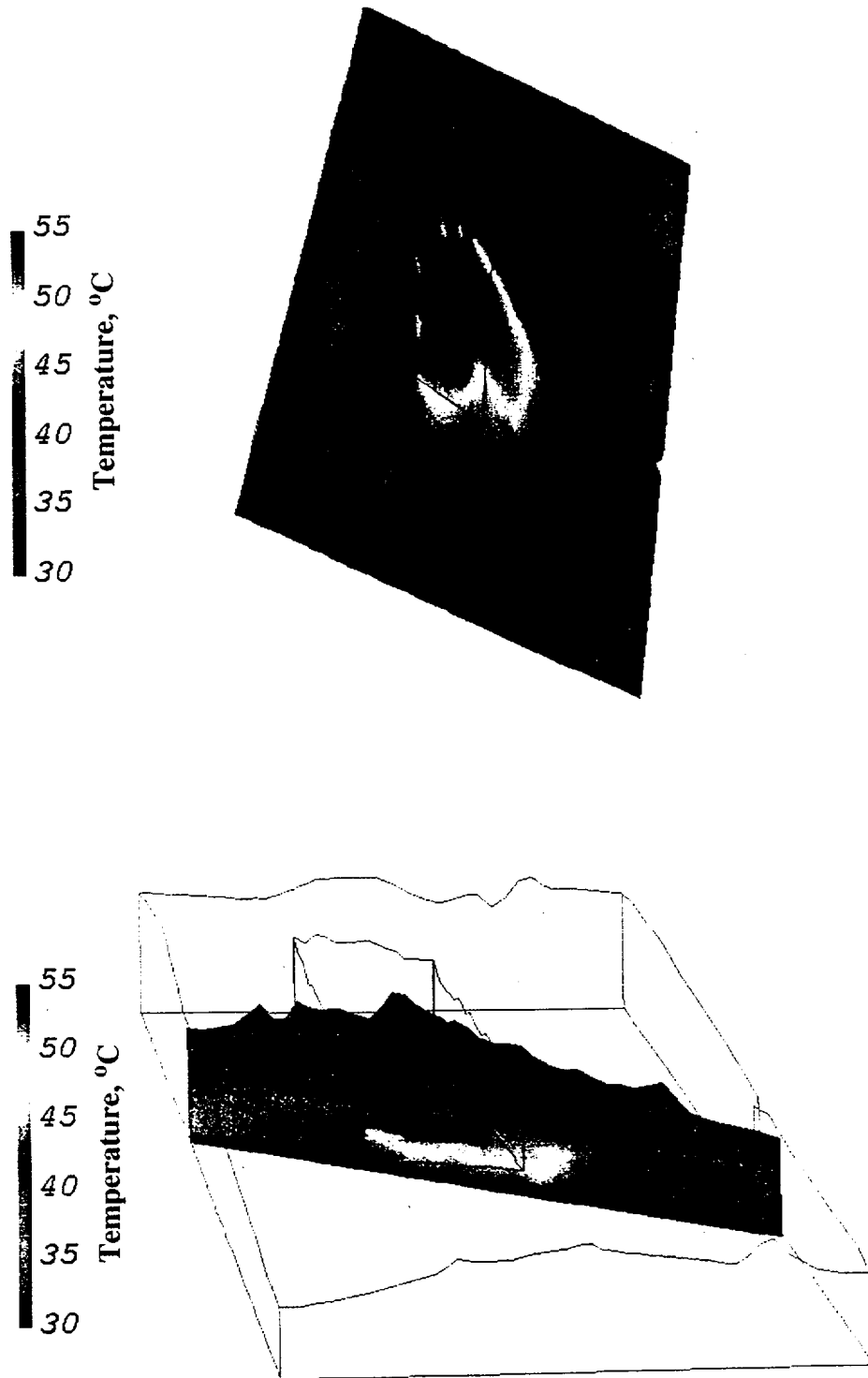


**Figure 6-29.** Temperature within the subsite-scale model domain after 30 ky of heat applied at the footprint of the repository. Top figure: horizontal profile at the water table. Bottom figure: vertical slice in the approximate direction of fluid flow. North is at the top of the figure.

## Transport Results

of heat with the prevailing groundwater flow. The bottom figure shows a vertical slice along the primary flow direction. Heat travels downward by conduction and laterally by advective transport with the flowing fluid.

The influence of this perturbation on transport of  $^{99}\text{Tc}$  is now discussed. For this simulation, we use the water table breakthrough curve for  $^{99}\text{Tc}$  presented as the dotted curve in Figure 6-19 as the input function and simulate  $^{99}\text{Tc}$  migration in the saturated zone during the evolution of the thermal/hydrologic flow field. The results are presented in Figure 6-30, a plot of

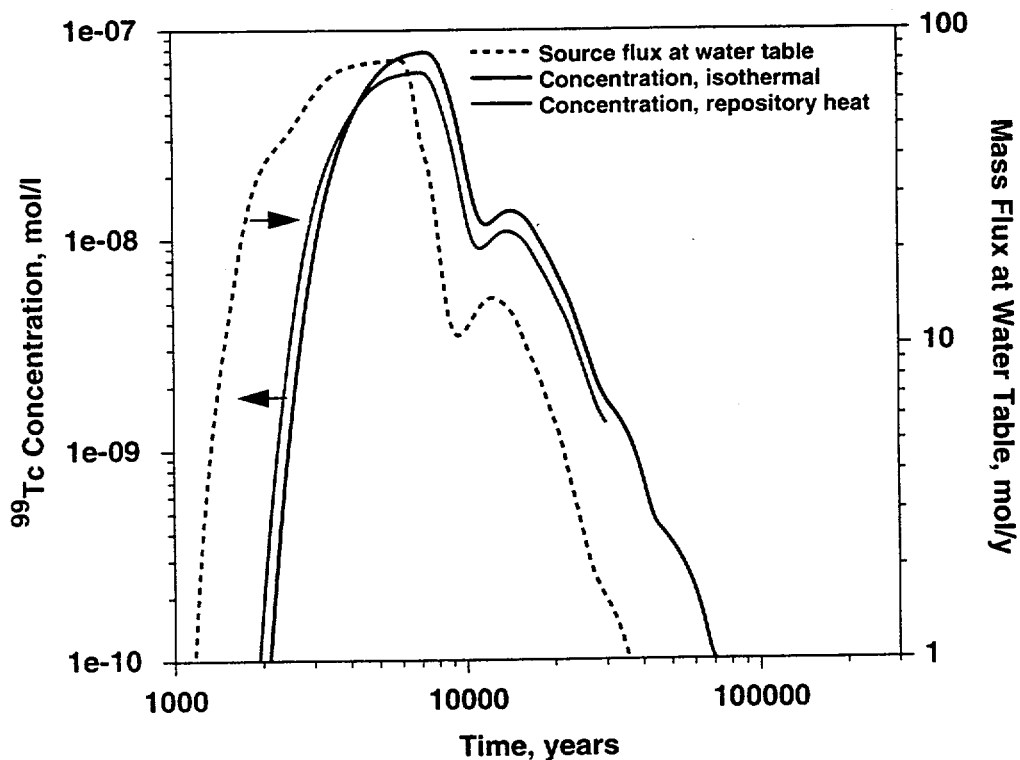


**Figure 6-30.**  $^{99}\text{Tc}$  breakthrough curve at the 5-km center-of-mass location of the subsite-scale model, comparing isothermal and thermally perturbed cases. Also shown is the mass flux at the water table used as input to the saturated-zone calculation for both cases.

concentration versus time at the 5-km center-of-mass location for the thermal and isothermal cases. The influence of repository heat on transport is quite small, and probably due to differences in the viscosity of the fluid.

Based on this analysis, we tentatively conclude that radionuclide migration through the saturated zone is minimally affected by repository heat. One aspect of repository heat that has not been treated here is the possibility of dynamic or permanent changes to the permeability and porosity of the saturated zone due to rock dissolution/precipitation processes. This aspect of saturated-zone performance was treated by Ho et al. (1996), who also tentatively conclude that the effects are likely to be small. However, definitive conclusions have not yet been reached on the impact of rock-water interactions. If these effects are also small, then we may conclude that saturated-zone radionuclide transport can be adequately simulated using models under ambient, pre-waste-emplacement conditions.

### **6.13 Integrated Unsaturated/Saturated-Zone Transport Predictions**

---

Now that the fundamental aspects of transport at the subsite scale and site scale have been established, we now present radionuclide transport predictions to the 5-km boundary for the key radionuclides  $^{99}\text{Tc}$ ,  $^{237}\text{Np}$ , and plutonium. As shown in Section 6.9, to predict concentration time histories, we need to couple the unsaturated-zone transport model predictions of mass flux at the water table versus time with the generic transport response curve that characterizes saturated-zone flow and transport. The convolution method described in Section 6.9 is used for this coupling.

The performance of the unsaturated zone with respect to the radionuclides listed above was studied in detail by Robinson et al. (1997), including evaluations of radionuclide solubilities and speciation based on Triay et al. (1997). The unsaturated-zone breakthrough curves at the water table are derived from that study. For  $^{99}\text{Tc}$  and  $^{237}\text{Np}$ , the impact of different climate scenarios on unsaturated-zone performance is through the percolation flux through the unsaturated zone. In general, higher percolation fluxes result in more rapid breakthrough at the water table due to the increased infiltration rate and, more importantly, the greater tendency for fracture bypassing of sorptive matrix minerals such as zeolites. For the purposes of the present study, each climate scenario results in a different unsaturated-zone percolation flux and, hence, a different radionuclide

breakthrough curve at the water table. In this section, we examine the role of the saturated zone in diluting the unsaturated-zone source term under different climate scenarios.

The situation for plutonium is somewhat different in that the key uncertainty, rather than climate scenario, is the possibility of colloid-facilitated transport. Robinson et al. (1997) show that if plutonium is primarily present in the aqueous phase (not sorbed to colloids), then the large measured sorption coefficients retard its migration very effectively. However, if most of the plutonium transports on colloids, transport times are much shorter and mass fluxes are greater. Therefore, in the section below on plutonium, the role of the colloid partitioning-coefficient  $K_c$  is studied. This factor defines the extent to which plutonium resides on colloid particles, that is,  $K_c$  is the mass of plutonium on colloids divided by the mass present in the aqueous phase.

### 6.13.1 $^{99}\text{Tc}$ Transport Predictions

The mass-flux breakthrough curves at the water table for  $^{99}\text{Tc}$  as a function of infiltration rate are shown in Figure 6-31. These results are obtained from the unsaturated-zone flow and transport model of Robinson et al. (1997). Details of the model assumptions that give rise to these results are documented in that milestone. These mass fluxes become the source term for saturated-zone model predictions, shown for the 5-km center-of-mass location of the subsite-scale model in Figure 6-32. The general shape of the water-table breakthrough curve is preserved in the concentration history at the downstream location. Peak concentrations are a function of the infiltration-rate scenario, which in turn influences the mass flux at the water table. The saturated zone dilutes this downward percolating fluid, but in essence, all cases are diluted by the same amount. Therefore, the performance degradation of the unsaturated-zone barrier due to the higher infiltration rate is reflected downstream in a higher concentration.

### 6.13.2 $^{237}\text{Np}$ Transport Predictions

A similar presentation will now be made for  $^{237}\text{Np}$ . Figure 6-33 shows the mass flux breakthrough at the water table, and Figure 6-34 is the corresponding concentration breakthrough at the 5-km center-of-mass location of the subsite-scale model. As was the case with  $^{99}\text{Tc}$ , the

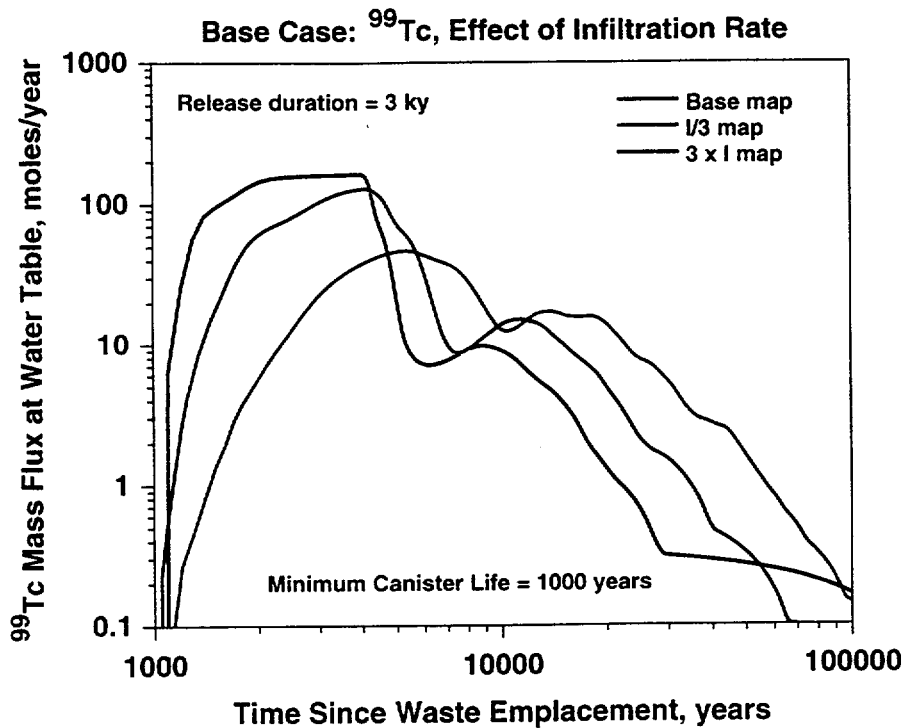


**Figure 6-31.** <sup>99</sup>Tc mass flux at the water table versus time for different infiltration scenarios. Predictions from Robinson et al. (1997).

shape of the mass-flux breakthrough at the water table, after dilution, is preserved in the prediction of concentration within the saturated zone. The dominant feature of these simulations is, therefore, the bypassing of the unsaturated zone through fractures, as was predicted by the unsaturated-zone transport model. For higher infiltration scenarios, this bypassing is more pronounced, and the overall prediction of total system performance is affected as a result. An additional simulation in Figure 6-34 shows the influence of saturated-zone sorption on zeolitic tuffs (the dotted curve). Even moderate sorption coefficients in the saturated zone give rise to considerable retardation, in this case, to times greater than 10 ky. Thus, sorption of <sup>237</sup>Np and other radionuclides in the saturated zone could have an important impact on total system performance.

### 6.13.3 Plutonium Transport Predictions

In Section 5.7, we present a model for colloid-facilitated transport of highly sorbing radionuclides such as plutonium. In Robinson et al. (1997), plutonium breakthrough curves at the

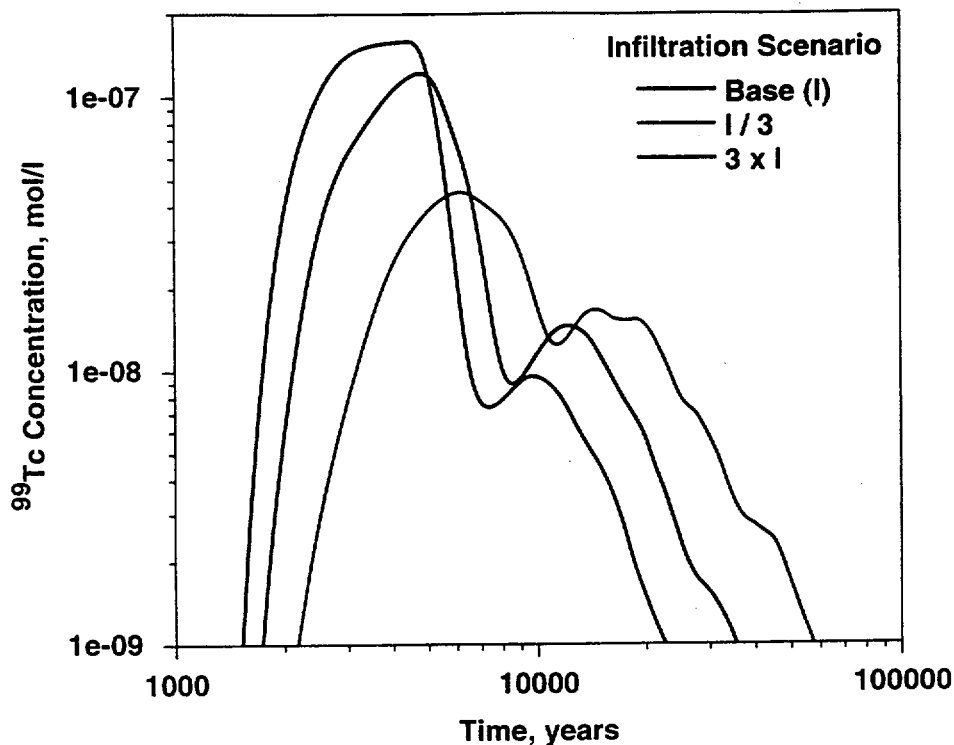


**Figure 6-32.**  $^{99}\text{Tc}$  concentration versus time at the 5-km center-of-mass location for different infiltration scenarios. Mass-flux inputs at the water table are shown in the previous figure.

water table were computed for various values of  $K_c$ , the partitioning coefficient of plutonium onto colloids. Figure 6-35, from Robinson et al. (1997), plots the mass-flux breakthrough at the water table for different values of  $K_c$ . For increasing values of  $K_c$ , the mass flux at the water table shifts to earlier time, and the peak value is much greater. With this parameter exerting such an overriding influence on the response, we expect that the saturated zone itself to change the model results very little. Figure 6-36 demonstrates this to be the case, in that the predicted concentration at the downstream location is simply a reflection of the mass flux of plutonium at the water table after mixing of the unsaturated-zone and saturated-zone fluids. In this simulation, we assumed a low effective porosity in the saturated zone due to exclusion of mobile colloids from the matrix rock. We also assumed that the colloids are fully mobile in the fractures and that filtration or attachment of colloids to the fracture surfaces are negligible. If our understanding of plutonium sorption to colloids continues to remain uncertain, then another avenue toward lowering the uncertainty

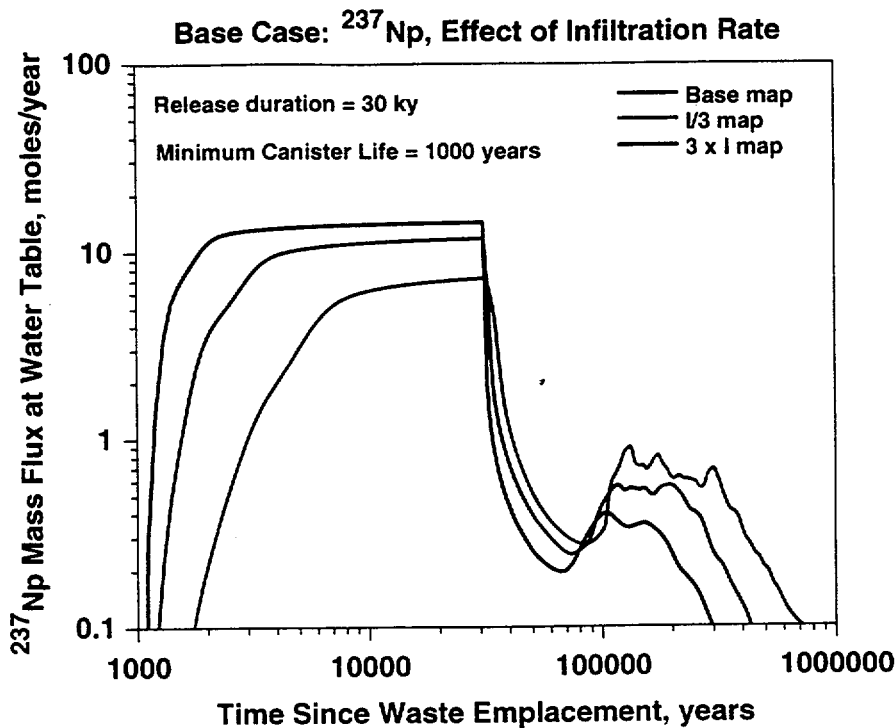


Figure 6-33.  $^{237}\text{Np}$  mass flux at the water table versus time for different infiltration scenarios. Predictions from Robinson et al. (1997).

bounds on plutonium transport is to use results from the C-Wells and other transport tests to include a filtration term for colloid transport through the fractured tuffs. Such a mechanism, if validated experimentally, would increase predicted travel times and reduce concentration levels.

## 6.14 Site-Scale Radionuclide Transport Predictions

In this section, we combine the results from the subsite-scale and site-scale models into a single, integrated set of radionuclide transport predictions from the repository to a presumed 20-km accessible-environment compliance point. The methodology is summarized in the following steps:

- Compute a radionuclide mass-flux breakthrough curve at the water table using the unsaturated-zone transport model (Robinson et al., 1997).

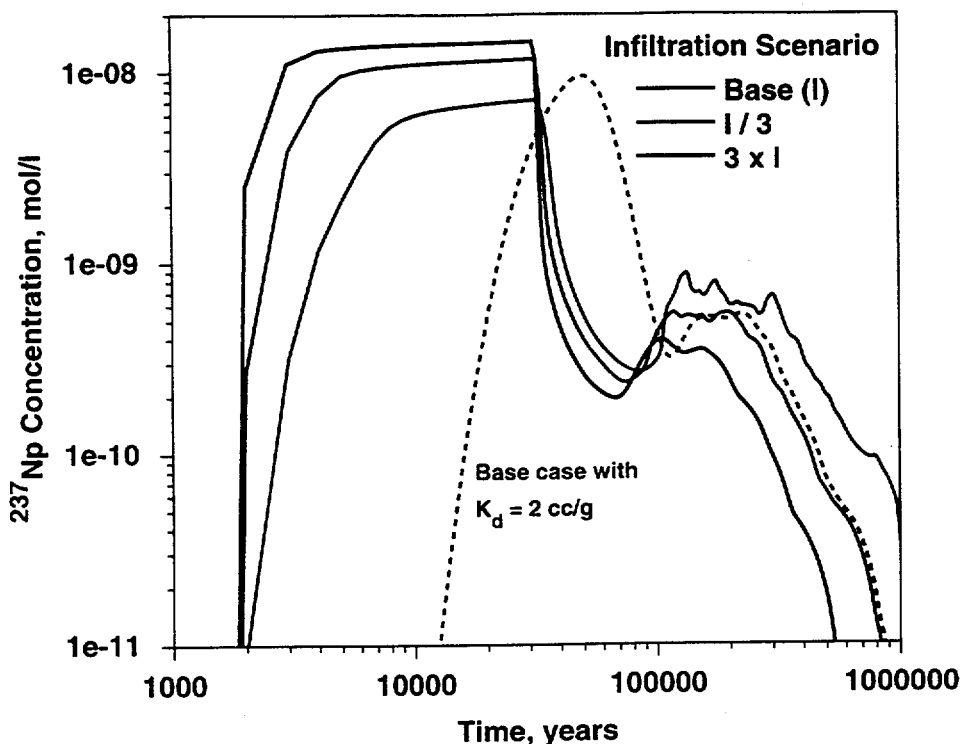


Figure 6-34.  $^{237}\text{Np}$  concentration versus time at the 5-km center-of-mass location for different infiltration scenarios. Mass-flux inputs at the water table are shown in the previous figure.

- Use the sub-site scale flow and transport model to predict the mass flux versus time exiting the subsite-scale model domain. In addition, record the concentration versus time at the 5-km compliance point at which the plateau concentration of the generic breakthrough curve simulation is the highest.
- Perform a generic breakthrough-curve calculation with the site-scale model for breakthrough at the 20-km compliance point and determine the location where the plateau concentration is highest. These results were presented previously in Section 6.8.
- Use numerical convolution to compute the concentration versus time curve at this location in response to the mass-flux input from the subsite-scale model.

This process is somewhat more cumbersome than if a single saturated-zone model were used for all of the calculations, but in the short term, it provides a suitable platform on which to examine saturated-zone transport issues. In the next version of the site-scale model, the geologic

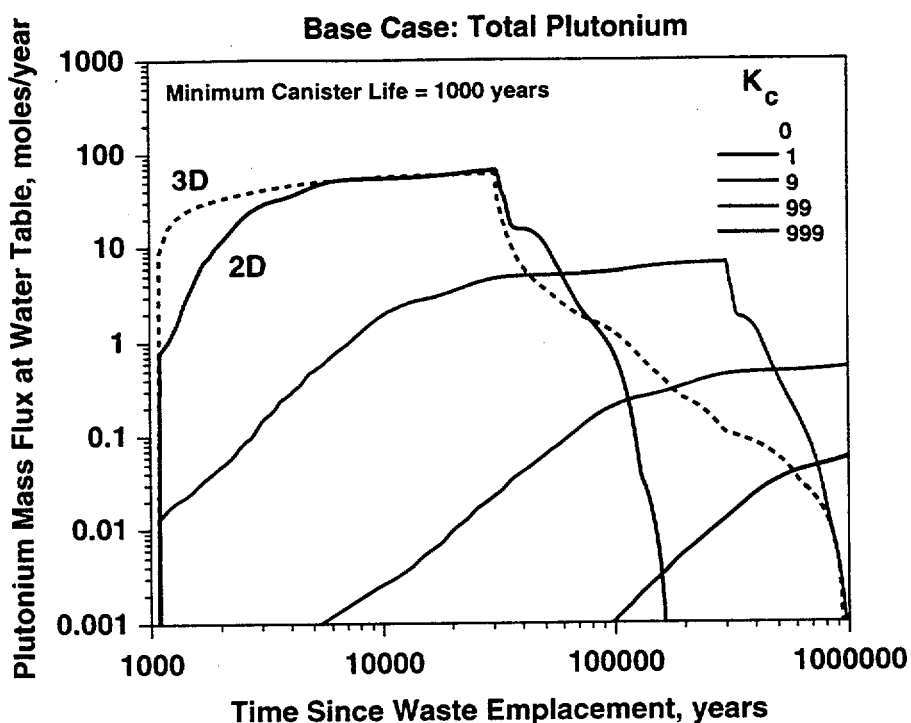


Figure 6-35. Plutonium mass flux at the water table versus time for different values of  $K_c$ . Predictions from Robinson et al. (1997).

stratigraphy near Yucca Mountain will be improved, and a single saturated-zone calculation will replace the two-step calculation process used here.

For these simulations, we take the unsaturated-zone water-table breakthrough curve used earlier for  $^{99}\text{Tc}$ , shown in Figure 6-19. The subsite-scale model calculation out to 5 km is also presented in this figure. This plot provided a good picture of saturated-zone performance out to a hypothetical 5-km compliance point, and by comparing the results to a 20-km location, we can illustrate the influence of the more distant compliance point on performance. The model output mass-flux curve for this simulation (used as input to the next calculation) is shown in Figure 6-37.

We now examine the convolution results of saturated-zone performance at 20 km for various site-scale model transport assumptions described earlier. Figure 6-38 shows the concentration versus time predicted at the 20-km location, along with the results at 5 km. The curves at 20 km are all for a point located in the centroid of the solute plume determined earlier; in

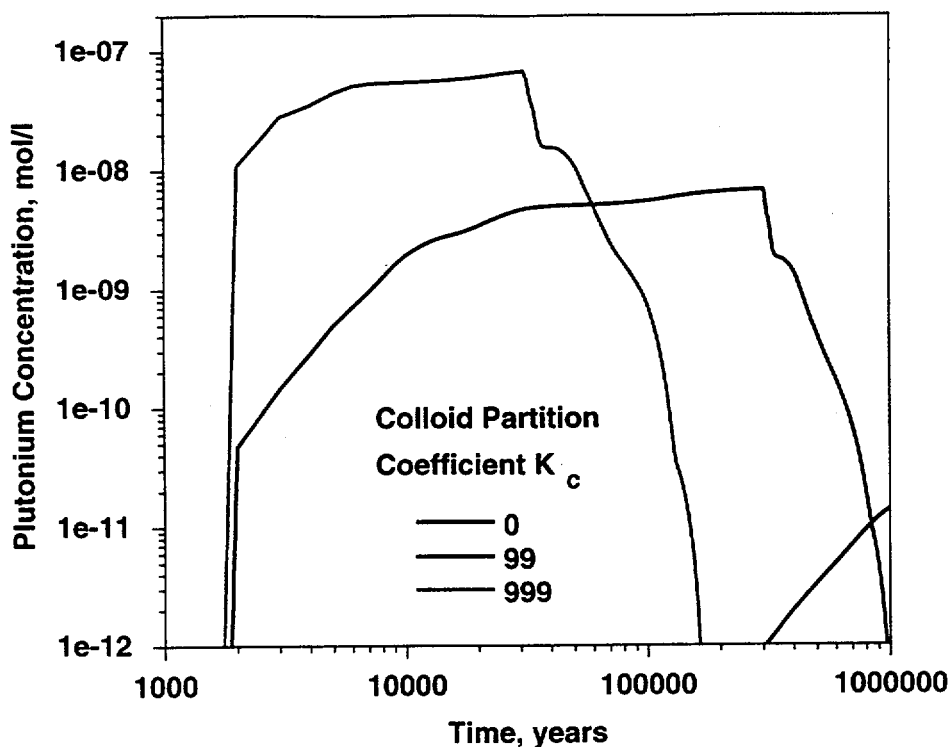
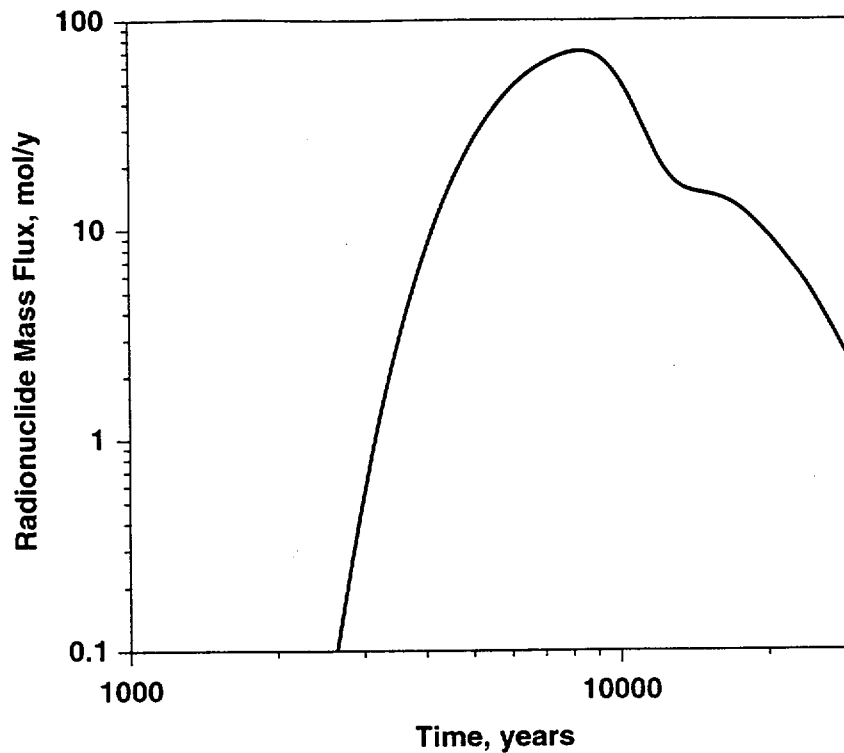


Figure 6-36. Plutonium concentration versus time at the 5-km center-of-mass location for different values of  $K_c$ . Mass flux inputs at the water table are shown in the previous figure.

the southwest portion of the model, downgradient from Yucca Mountain. The curve labeled “fracture porosity” assumed a low value in the fractures for all tuff and carbonate rocks with high values only in the alluvium. The travel time delay relative to the curve at 5 km is on the order of 10 ky, according to the site-scale model results. The travel time for this simulation is dominated by transport through the alluvium, because travel times in fractured rock are very short with the assumed transport porosity of  $10^{-4}$ . There is also a significant dilution effect due to dispersion at the downstream location. Dispersion of the plume transverse to the flow direction is the cause of the lower concentration at the more distant compliance point. The greater flow distance affords more time for heterogeneities to spread the radionuclide plume, and lower concentrations result. We caution that for this model, grid refinement was not applied along the transport pathway; therefore, some numerical dispersion is likely to be present. A more accurate calculation on a refined grid will be performed on the next version of the site-scale model. Nonetheless, the trends



**Figure 6-37.**  $^{99}\text{Tc}$  mass flux exiting the subsite-scale model. This curve is input to the site-scale model at the appropriate location.

with increasing flow path distance will be present, as it is a natural feature of transport in groundwater.

For the next curve, marked “matrix porosity,” we assumed that matrix diffusion in the fractured rock units was pervasive enough for the effective porosity to equal the fracture porosity. This assumption increases the travel times in the fractured rock units, pushing the time for the peak concentration to about 40 ky from a value of less than 20 ky for the fracture-porosity case. The peak concentration is also reduced significantly relative to the fracture-porosity curve.

Finally, even a small amount of sorption in the alluvium ( $K_d = 1 \text{ cc/g}$ ) delays the arrival dramatically and reduces the peak by roughly an order of magnitude relative to the fracture porosity case. The benefits of sorption are maximized when there is full contact of the radionuclides with sorptive minerals. This is most likely the case for porous flow through alluvium. Although heterogeneities are sure to exist in this medium, it is less likely that severe

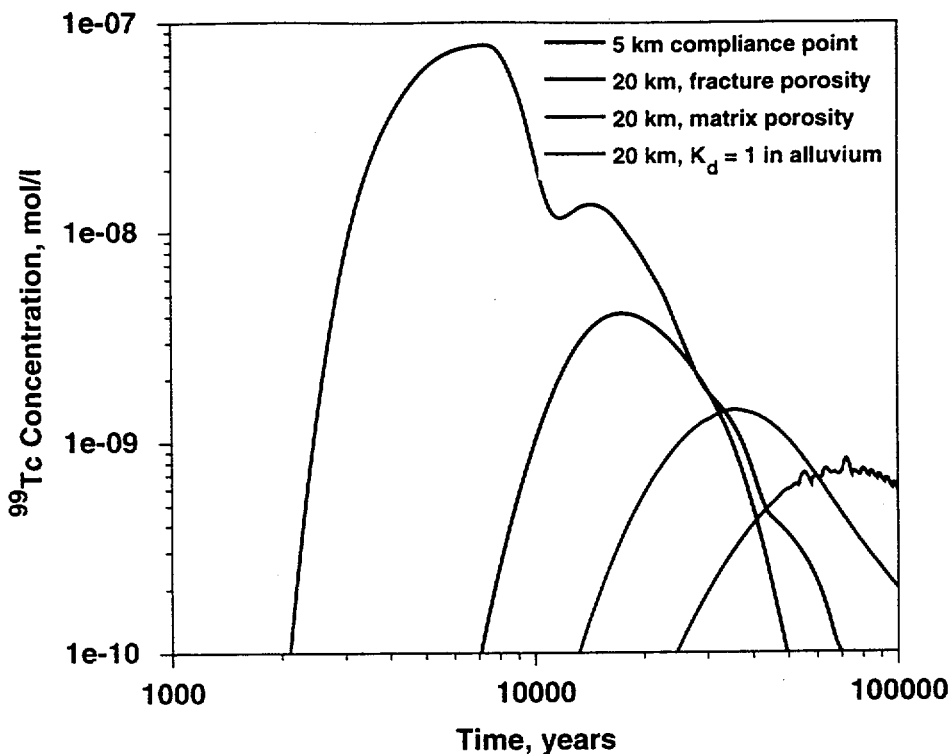


**Figure 6-38.** Comparison of  $^{99}\text{Tc}$  breakthrough curves at the compliance point of the site-scale model for different transport parameter assumptions. Source term shown in Figure 6-37.

channeling and bypassing of sorptive sites would occur in a porous medium, at least compared to flow through fractured rock. Therefore, under a 20-km or greater compliance regulatory criterion, characterizing radionuclide sorption onto the alluvium in locations of the predicted transport pathways is critical to improving our estimates of site performance. The benefits to performance of even a small amount of sorption are potentially enormous.

### 6.15 Dual-Porosity Modeling

One of the key uncertainties in unsaturated-zone flow and transport in fractured rock is the conceptual model for interactions between the fractures and surrounding matrix blocks. With regard to flow issues, it is well-known (e.g., Warren and Root, 1963) that in well tests, even though the fractures contribute almost exclusively to the bulk permeability of the medium, matrix storage effects impact the pressure response curves. These are transient effects that are important to

consider when interpreting well tests. At the scale of the flow models considered in the present study, transients due to long-term changes in forcing conditions (head or flux boundary conditions) would also contribute to the response of the system. However, at steady state, it can be shown that the flow field does not depend on the porosity of the medium. From these considerations, it follows that a dual-porosity model, in which large-scale permeability is controlled by fractures but fluid storage is controlled by the matrix porosity, will yield identical results to a single-continuum case.

The situation for solute transport is more complex, however. Transport of a solute, even for a steady-state flow field, is inherently a transient process. If solute cannot diffuse fully into the rock matrix during its transit through a fractured medium, then interactions between the fractures and matrix control the breakthrough curve. In the development of the conceptual model for transport (Chapter 5) and its implementation as an effective porosity for transport in Section 6.10, we showed that this transport porosity spans the range from fracture porosity (on the order of  $10^{-4}$ ) to matrix porosity (0.1–0.3). In this section, we expand on this concept by developing models that relax the assumption that a single porosity must be used to characterize transport through fractured rock. We formulate a dual-porosity transport model using the subsite-scale model in two ways:

- use the continuum-flow simulation with low fracture porosity but use the matrix-diffusion model of the particle-tracking module of FEHM to simulate dual-porosity transport; and
- develop a dual-porosity flow and transport simulation with transport computed using the finite-element solution to the advection-dispersion equation.

These two approaches are presented in the subsections that follow.

### 6.15.1 Dual-porosity transport with particle tracking

Figure 6-39 shows the results of a breakthrough-curve simulation using the subsite-scale model with a fracture porosity of  $10^{-4}$  in all units for different values of the diffusion coefficient. The curves are plots of the cumulative mass leaving the model domain versus time for a pulse of

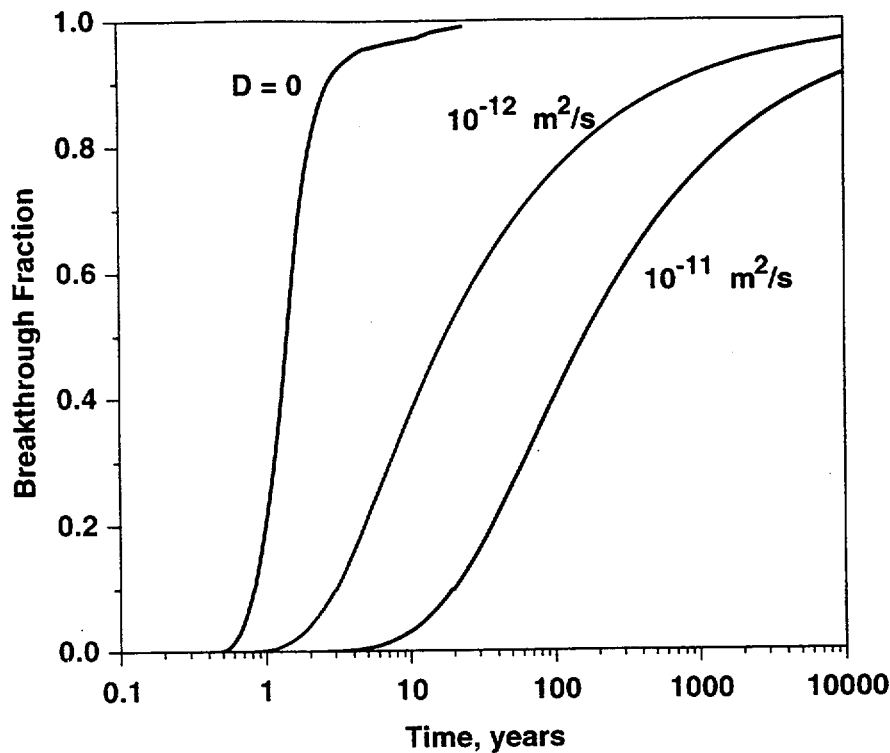


**Figure 6-39.** Comparison of breakthrough curves at the 5-km center-of-mass location of the sub-site-scale model for different values of the matrix diffusion coefficient. The particle-tracking model is used.

solute injected at time  $t = 0$ . For all cases, the fracture half-spacing is assumed to be 10 m. For the case in which the extent of matrix diffusion is relatively small, such that the radionuclide has insufficient time to diffuse fully between fractures, the model result mimics the results presented in the conceptual model development in that matrix diffusion results in an effective travel time delay relative to fracture-dominated transport. However, for the case in which diffusion coefficients are high enough, or fracture spacings are small enough, the assumption in the particle-tracking technique (transport in individual, noninteracting fractures) breaks down, and the solutions no longer provide an adequate prediction of transport. For this set of simulations, the diffusion coefficient of  $10^{-11} \text{ m}^2/\text{s}$  is about the point at which the assumption is violated. This result compares to values of 1 to  $4 \times 10^{-11} \text{ m}^2/\text{s}$  for  $^{99}\text{Tc}$  reported by Triay et al. (1997). For smaller values, the curves shown in this simulation reflect a valid calculation using the matrix-diffusion model.

There is probably a range of parameter values consistent with the conceptual model of radionuclide transport for which a particle-tracking simulation such as those in Figure 6-39 would yield accurate simulation results. Unfortunately, one of the key transport mechanisms likely to be relevant to saturated-zone transport, lateral diffusion, is not present in the particle-tracking model. Therefore, the model as currently constituted is not appropriate for large-scale simulations. We, therefore, must use the finite-element solution, despite the computational efficiency of the particle-tracking module.

### 6.15.2 Dual-porosity flow and transport with the finite-element solution

In this section, we describe the results of a series of flow and transport simulations using the finite-element flow and transport module of FEHM. This approach first requires a recalculation of the flow field in dual-porosity mode. This calculation on the subsite-scale model yielded a steady-state pressure field that was indistinguishable from the continuum results presented in Section 6.6. Furthermore, the fluid mass flux through the model domain agreed to within seven decimal places with the value for the single continuum. This result was expected, for reasons discussed earlier. The dual-porosity calculations were performed with fracture porosity equal to  $10^{-4}$  at all locations and matrix porosities equal to the values cited in Table 6-2. The key parameters affecting the transport results are the mean fracture spacing and the diffusion coefficient.

Figure 6-40 shows the transport breakthrough curves at location b for various diffusion coefficients and a fracture spacing of 10 m. With no matrix diffusion, the breakthrough curve is dominated by fracture flow and transport, and short times are predicted. At the other extreme, long transport times result from a high value of the diffusion coefficient. For this case, it takes an unrealistically large diffusion coefficient to reach the limit of matrix-like transport porosity (the red curve,  $D = 10^{-8}$ ), but we present the curve to illustrate the ability of the dual-porosity model to capture this limit. At intermediate diffusion, the model predicts intermediate results in terms of the mean travel time. However, the model fails to capture the transport process accurately for values

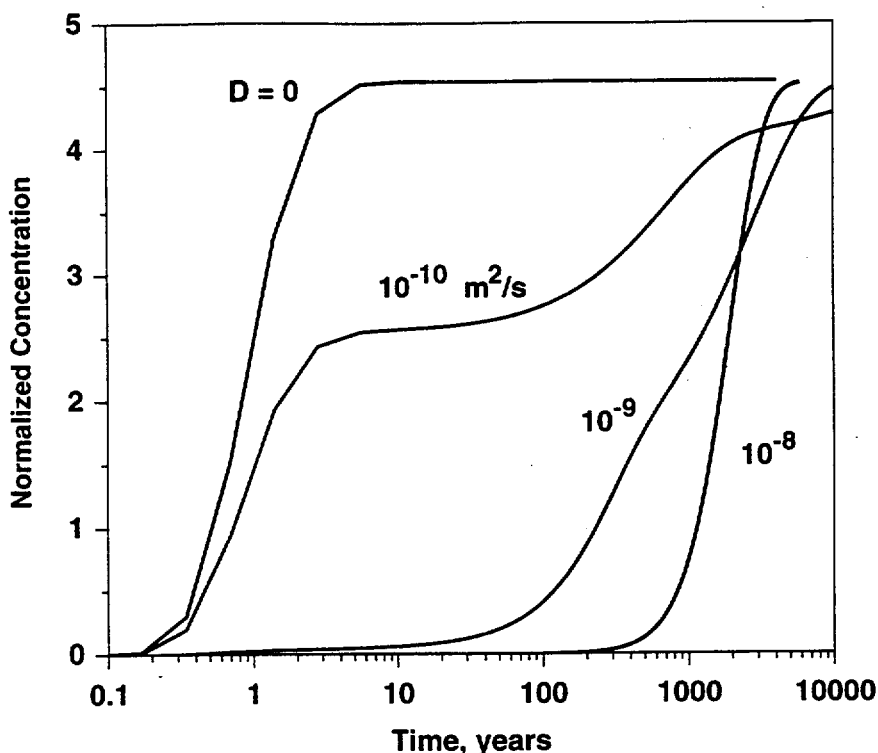


**Figure 6-40.** Comparison of breakthrough curves at the 5-km center-of-mass location of the subsite-scale model for different values of the matrix diffusion coefficient. The dual-porosity transport model is used.

of the diffusion coefficient for which diffusion is only a short distance into the rock matrix, such as the  $10^{-10} \text{ m}^2/\text{s}$  case. The bi-modal breakthrough curve is unrealistic, because the actual system, better characterized by the particle-tracking algorithm for this case, exhibits a smooth rise to the final concentration. The FEHM dual-porosity model has two grid points into the matrix, which is insufficient to capture a sharp concentration gradient. Thus, the dual-porosity model can capture the two extremes of matrix diffusion but fails to yield realistic results for intermediate amounts of diffusion.

The question of which type of model to use for performance predictions must be addressed in the context of the key uncertainties in the flow and transport model. Given the level of uncertainty in matrix-diffusion and fracture-spacing properties and the general similarity in the continuum and dual-porosity models at the extremes of diffusion coefficient, it is probably sufficient to use a single continuum with a transport porosity adjusted based on flow velocity,

## Transport Results

---

diffusion parameters, and fracture spacing to yield the "correct" mean breakthrough time at the compliance point. This statement is especially true for more distant compliance points, such as the hypothetical 20-km point assumed in this study. The breakthrough time, in addition to the dispersivity, are the key model outputs controlling the performance of the saturated-zone transport system. Therefore, an abstracted continuum model that preserves the large-scale flow patterns predicted by the flow model, yet also estimates the breakthrough time and dispersive characteristics correctly, should capture the essential features of the saturated-zone flow and transport barrier.

### 6.16 Conclusions

---

Several models and numerical techniques were used to obtain results for radionuclide transport in the saturated zone. A convolution integral method was described that links unsaturated-zone radionuclide release with saturated-zone flow. This method allows many different radionuclide release scenarios to be investigated with only a few computer runs. The validity of the technique was established by comparison with full-scale simulations. Sensitivity studies were performed on several key parameters, including dispersivity and the sorption coefficient  $K_d$ . In general, the saturated zone provides an important component in a "defense-in-depth" strategy in which uncertainties leading to poor performance in one part of the repository system are mitigated by the performance of another radionuclide transport barrier.

The impact of repository heat on radionuclide transport was also examined and found to be of minor importance. Some additional effort should be spent in investigation of temperature-dependent rock-water interactions, as this could result in permanent changes in porosity and permeability in the saturated zone.

A transport model using a combination of subsite-scale and site-scale models, and under conditions in which the effective porosity is the matrix porosity, produced transport times to a hypothetical 5-km compliance point on the order of a few thousand years. The result is sensitive

## Transport Results

---

to the amount of matrix diffusion used. Transport times to the 20-km compliance point varied between 10 ky and 50 ky depending on assumptions regarding fracture and alluvium properties.

Equivalent-continuum and dual-porosity models were investigated to determine their usefulness in representing transport in fractured tuffs. The results show that an appropriate abstracted transport model would employ the effective porosity concept with theoretical relationships involving matrix-diffusion and fracture-spacing parameters used to set the transport porosity throughout the model domain.

# Chapter 7 - Conclusions and Recommendations

In this study, a combination of flow models was necessary to simulate transport from the repository to various compliance boundaries. The flow models used in this report were provided by the USGS and Sandia National Laboratories. The USGS model used was the most recently calibrated site-scale model and includes a correction from a version of two months ago that results in reasonable flux values on the model boundaries. Due to coarse sampling (1500 m), the region under the repository overpredicted travel times to the accessible environment. To resolve this problem, a subsite-scale model with finer sampling (250 m) was used in the vicinity of Yucca Mountain. The radionuclide flux from this model was applied to the site-scale model to produce travel times to the 20-km compliance point.

Grid resolution was found to be critical for both flow and transport. The ability to resolve heterogeneous geologic units was a function of grid resolution. Grid resolution studies were carried out with both unstructured and structured grids. It was found that the USGS calibrated flow model produced fluxes that changed little by resolving the grid and was thus deemed of sufficient resolution for flow simulation. New methods were described to locally resolve grids for transport simulations.

The FEHM code proved to be an efficient and flexible tool for obtaining flow and transport solutions in the YMP site-scale saturated zone. Modifications were made to FEHM to provide a seamless link to the parameter-estimation code PEST.

A conceptual model was described that includes advective transport of radionuclides, dispersion, diffusion of radionuclides from fractures into the rock matrix, and sorption. Within the fractured tuffs, the migration of radionuclides is expected to be primarily through regions with higher bulk fracture permeability. Flow within individual joints probably occurs through channels rather than as sheet flow through parallel-plate fractures. At more distant downstream locations, the migration is likely to be through alluvium, and a model for flow and transport through a porous continuum, rather than a fractured rock, is likely to apply. It was shown that transport can be

## Conclusions and Recommendations

---

approximated using an effective transport porosity that, in general, falls between the fracture porosity and the porosity of the surrounding rock matrix. Dispersion is caused by heterogeneities at all scales from the pore scale to the scale of the thickness of individual strata and the length of structural features such as faults. The resulting spreading of radionuclides is important to performance and must be captured in transport models. Only the largest heterogeneities are represented explicitly in the site-scale model; all dispersion caused by smaller-scale features must be represented through the use of a dispersion model.

Several models and numerical techniques were used to obtain results for radionuclide transport in the saturated zone. A convolution integral method was described that links unsaturated-zone radionuclide release with saturated-zone flow. This method allows many different radionuclide release scenarios to be investigated with only a few computer runs. The validity of the technique was established by comparison with full-scale simulations. Sensitivity studies were performed on several key parameters, including dispersivity and the sorption coefficient  $K_d$ . In general, the saturated zone provides an important component in a "defense-in-depth" strategy in which uncertainties leading to poor performance in one part of the repository system are mitigated by the performance of another radionuclide transport barrier.

The impact of repository heat on radionuclide transport was also examined and found to be of minor importance. Some additional effort should be spent in investigation of temperature-dependent rock-water interactions, as this could result in permanent changes in porosity and permeability in the saturated zone.

A transport model using a combination of subsite-scale and site-scale models produced, under conditions in which the effective porosity is the matrix porosity, transport times to a hypothetical 5-km compliance point on the order of a few thousand years. The result is sensitive to the amount of matrix diffusion used. Transport times to the 20-km compliance point varied between 10 ky and 50 ky depending on assumptions regarding fracture and alluvium properties.

## Conclusions and Recommendations

---

Equivalent-continuum and dual-porosity models were investigated to determine their usefulness in representing transport in fractured tuffs. The results show that an appropriate abstracted transport model would employ the effective-porosity concept with theoretical relationships involving matrix diffusion and fracture-spacing parameters used to set the transport porosity throughout the model domain.

We recommend the following future activities:

- Continue close collaboration with the USGS flow modeling effort. Continue to update the Stratigraphic Framework Model (SFM) with the best available data and establish quantitative measures of grid fidelity to the SFM.
- Perform preliminary transport simulations during flow calibration efforts. This effort will uncover early possible incompatibilities between the flow and transport conceptual models and will eliminate any problems in sampling frequency that may result in an inaccurate representation of units. This parallel computation may also uncover potential fast paths for radionuclides that can be corroborated or dismissed with supporting thermal or geochemical data. In this way, transport modeling will provide a worth-of-effort tool for improving the flow model. By establishing the effect on the radionuclide flux at the compliance boundaries, flow model improvements, such as creating a detailed inlet flux map, may be evaluated with respect to its importance to performance assessment.
- Enlarge the modeling domain of the site-scale model north of the large hydraulic gradient area where the calibration of the regional model is better and the fluxes of the regional model are more defensible. This approach will also allow better redistribution of fluxes from the three-layer regional model to the sixteen-layer site-scale model.
- Use the 250-m sampling of the SFM. This effort will provide sufficient resolution, in the vicinity of Yucca Mountain, for transport calculations.
- Use the stochastic transport modeling to better characterize uncertainties in the dispersive mixing process occurring at subgrid block scales.

## Chapter 8 - References

- Altman, S. J., B. W. Arnold, C. K. Ho, S. A. McKenna, R. W. Barnard, G. E. Barr, and R. E. Eaton. 1996. Flow calculations for Yucca Mountain groundwater travel time (GWTT-95). Sandia National Laboratory technical report SAND96-0819.
- Arya, A. 1986. Dispersion and reservoir heterogeneity. Ph.D. Dissertation. University of Texas, Austin.
- Benson, L. V., J. H. Robison, R. K. Blankennagel, and A. E. Ogard. 1983. Chemical composition of groundwater and the location of permeable zones in the Yucca Mountain Area, Nevada. U.S. Geological Survey open file report 83-854.
- Brown, S. R. 1987. Fluid flow through rock joints: The effect of surface roughness. *Journal of Geophysical Research* 92(B2): 1337-1347.
- Buesch, D. C., R. W. Spengler, T. C. Moyer, and J. K. Geslin. 1996. Revised stratigraphic nomenclature and macroscopic identification of lithostratigraphic units of the Paintbrush Group exposed at Yucca Mountain, Nevada. U.S. Geological Survey open file report 94-496.
- Chipera, S. J., K. E. Carter Krogh, D. T. Vaniman, D. L. Dish, and J. W. Carey. 1997a. Preliminary three-dimensional mineralogical model of Yucca Mountain, Nevada. Los Alamos National Laboratory YMP milestone report SP321AM4.
- Chipera, S. J., D. T. Vaniman, D. L. Bish, and J. W. Carey. 1997b. Mineralogic variation in drill holes USW NRG-6, NRG-7/7a, SD-7, SD-9, SD-12, and UZ#14: New data from 1996-1997 analyses. Los Alamos National Laboratory YMP milestone report SP321BM4.
- Ciesnik, M. S. 1995. Groundwater altitudes and well data, Nye County, Nevada, and Inyo County, California. U.S. Geological Survey open file report 93-89.
- Clayton, R. W., W. P. Zelinski, and C. A. Rautman, (CRWMS). 1997. ISM 2.0: A 3-D geological framework and integrated site model of Yucca Mountain: Version ISM 1.0, Doc ID B00000000-01717-5700-00004, Rev. 0, MOL.19970122.0053. Civilian Radioactive Waste Management System Management and Operating Contractor (February).
- Czarnecki, J. B., C. C. Faunt, C. W. Gable, and G. A. Zyvoloski. 1997. Preliminary three-dimensional finite-element groundwater flow model of the saturated zone, Yucca Mountain, Nevada. U.S. Geological Survey YMP milestone number SP23NM3.
- D'Agnese, F. A., C. C. Faunt, A. K. Turner, and M. C. Hill. 1997. Hydrogeologic evaluation and numerical simulation of the Death Valley regional groundwater flow system, Nevada and California, using geoscientific information systems. U.S. Geological Survey Water-Resources investigations report 96-4300 (in press),
- Dash, Z. V., and G. A. Zyvoloski. 1996a. Software design document for the FEHM application. Los Alamos National Laboratory YMP document FEHM SDD, ECD-22,
- Dash, Z. V., B. A. Robinson, and G. A. Zyvoloski. 1996b. V & V plan and procedures for the FEHM application. Los Alamos National Laboratory YMP document FEHM VVP, ECD-22.
- Dash, Z. V., B. A. Robinson, and G. A. Zyvoloski. 1996c. V & V report for the FEHM application. Los Alamos National Laboratory YMP document FEHM VVR, ECD-22.

## References

---

- Erickson, J. R., and R. K. Waddell. 1985. Identification and characterization of hydrologic properties of fractured tuff using hydraulic and tracer tests—test well USW H-4, Yucca Mountain, Nye County, Nevada. U.S. Geological Survey Water Resources investigations report 85-4066.
- Faunt, C. 1997. Personal communication. U.S. Geological Survey.
- Fung, L. S.-K., A. D. Hiebert, and L. X. Nghlem. 1992. Reservoir simulation with a control-volume finite-element method. *SPE Reservoir Eng.* (August): 349–357.
- Gable, C. W., T. A. Cherry, H. E. Trease, and G. A. Zyvoloski. 1995. GEOMESH grid generation. Los Alamos National Laboratory report LA-UR-95-4143.
- Gable, C. W., H. Trease, and T. Cherry. 1996. Geological applications of automatic grid generation tools for finite elements applied to porous flow modeling. In *Numerical Grid Generation in Computational Fluid Dynamics and Related Fields*, edited by B. K. Soni, J. F. Thompson, H. Hausser, and P. R. Eiseman, Engineering Research Center. Mississippi State University Press.
- Gelhar, L. W., A. Mantoglou, C. Welty, and K. R. Rehfeldt. 1985. A review of field-scale physical solute transport processes in saturated and unsaturated porous media. Report EPRI EA-4190, Project 2485-5, Electric Power Research Institute. Palo Alto, California.
- Gelhar, L. W. 1987. Applications of stochastic models to solute transport in fractured rocks. SKB technical report 87-05 (Swedish Nuclear Fuel and Waste Management Co., Stockholm, Sweden).
- Grisak, G. E., and J. F. Pickens. 1980. Solute transport through fractured media: 1. The effect of matrix diffusion. *Water Resources Research* 16(4): 719–730.
- Harr, L., J. Gallagher, and G. S. Kell. 1984. *NBS/NRC Steam Tables, Thermodynamics, and Transport Properties and Computer Programs for Vapor and Liquid States of Water*. Hemisphere Press.
- Ho, C. K., N. D. Francis, B. W. Arnold, Y. Xiang, S. A. McKenna, S. Mishra, G. E. Barr, S. J. Altman, X. H. Yang, and R. R. Eaton. 1996. Thermo-hydrologic modeling of the potential repository at Yucca Mountain including the effects of heterogeneities and alternative conceptual models of fractured porous media. Level-3 milestone T6536, submitted to U.S. Department of Energy.
- Karasaki, K., and D. Galloway. 1990. Method development and strategy for the characterization of complexly faulted and fractured rhyolitic tuffs, Yucca Mountain, Nevada, USA. In *Proceedings of the Nuclear Energy Agency Workshop on Flow Heterogeneity and Site Evaluation, SEDE '90, Paris, France*.
- Karasaki, K., M. Landsfeld, and K. Grossenbacher. 1990. Building a conceptual model at the UE25-C hole complex. In *Volume 2, Proceedings of International Topical Meeting: High Level Radioactive Waste Management, Las Vegas, Nevada*. American Society of Civil Engineers and American Nuclear Society.
- Lallemand-Barres, A., and P. Peaudecerf. 1978. Recherche des relations entre la valeur de la dispersivité macroscopique d'un aquifère, ses autres caractéristiques et les conditions de mesure. *Bull. Bur. Rech. Geol. Min.*, 3, 4.

## References

---

- Long, J. C. S., and D. M. Billaux. 1987. From field data to fracture network modeling: An example incorporating spatial structure. *Water Resources Research* 23(7): 1201–1216.
- Maloszewski, P., and A. Zuber. 1985. On the theory of tracer experiments in fissured rocks with a porous matrix. *Journal of Hydrology* 79: 333–358.
- Maloszewski, P., and A. Zuber. 1991. Influence of matrix diffusion and exchange reactions on radiocarbon ages in fissured carbonate aquifers. *Water Resources Research* 27(8): 1937–1945.
- Neretnicks, I. 1980. Diffusion in the rock matrix: An important factor in radionuclide migration? *Journal of Geophysical Research* 85(B8): 4379–4397.
- Neretnicks, I., T. Eriksen, and P. Tahtinen. 1982. Tracer movement in a single fissure in granitic rock: Some experimental results and their interpretation. *Water Resources Research* 18: 849–858.
- Neuman, S. P. 1990. Universal scaling of hydraulic conductivities and dispersivities in geologic media. *Water Resources Research* 26(8): 1749–1758.
- Peters, R. R., E. A. Klavetter, I. J. Hall, S. C. Blair, P. R. Heller, and G. W. Gee. 1984. Fracture and matrix hydrologic characteristics of tuffaceous materials from Yucca Mountain, Nye County, Nevada. Sandia National Laboratories report SAND84-1471.
- Pickens, J. F., and G. E. Grisak. 1981. Scale-dependent dispersion in a stratified granular aquifer. *Water Resources Research* 17(4): 1191–1211.
- Rasmuson, A., and I. Neretnicks. 1986. Radionuclide transport in fast channels in crystalline rock. *Water Resources Research* 22(8): 1247–1256.
- Reeves, M. 1994. Review and selection of unsaturated flow models. Intera document B00000000-01 425-2200-00001.
- Reimus, P. W., and H. J. Turin. 1997. Draft report of results of hydraulic and tracer tests at the C-wells complex. Los Alamos National Laboratory YMP milestone SP23APMD.
- Robinson, B.A. 1988. Fracture network modeling of a hot dry rock geothermal reservoir. In *Proceedings of the Thirteenth Workshop on Geothermal Reservoir Engineering, Stanford University*, pp. 211–218.
- Robinson, B. A. 1994. A strategy for validating a conceptual model for radionuclide migration in the saturated zone beneath Yucca Mountain. *Radioactive Waste Management and Environmental Restoration* 19: 73–96.
- Robinson, B.A., A.V. Wolfsberg, H.S. Viswanathan, C.W. Gable, G.A. Zyvoloski, and H.J Turin,. Modeling of flow, radionuclide migration, and environmental isotope distributions at Yucca Mountain, Los Alamos National Laboratory YMP Milestone 3672, 1996.
- Robinson, B. A., H. S. Viswanathan, A. V. Wolfsberg, G. W. Gable, and G. Bussod. 1997. The site-scale unsaturated zone transport model of Yucca Mountain. Los Alamos National Laboratory YMP Milestone SP25BMC.
- Stock, J. M., and J. H. Healy. 1988. Stress field at Yucca Mountain, Nevada. In *Geologic and Hydrologic Investigation of a Potential Nuclear Waste Disposal Site at Yucca Mountain, Southern Nevada, U.S.*, edited by M.D. Carr and Y.C. Yount, pp. 87–93. U.S. Geological Survey bulletin 1790.

## References

---

- Stock, J. M., J. H. Healy, and S. H. Hickman. 1984. Report on televiewer log and stress measurements in core hole USW G-2, Nevada Test Site, October–November, 1982. U.S. Geological Survey open file report 84-172.
- Stratigraphic Geocellular Modeling Reference Guide*. 1995. Landmark Graphics Corporation.
- Sudicky, E. A., and E. O. Frind. 1981. Carbon-14 dating of groundwater in confined aquifers: Implications of aquitard diffusion. *Water Resources Research* 17(4): 1060–1064.
- Sudicky, E. A., R. W. Gillham, and E. O. Frind. 1985. Experimental investigation of solute transport in stratified porous media: 1. The nonreactive case. *Water Resources Research* 21(7): 1035–1041.
- Tang, D. H., E. O. Frind, and E. A. Sudicky. 1981. Contaminant transport in fractured porous media: Analytical solution for a single fracture. *Water Resources Research* 17(3): 555–564.
- Trease, H., D. George, C. W. Gable, J. Fowler, A. Kuprat, and A. Khamyaseh. 1996. The X3D grid generation system. In *Numerical Grid Generation in Computational Fluid Dynamics and Related Fields*, edited by B. K. Soni, J. F. Thompson, H. Hausser, and P. R. Eiseman, Engineering Research Center. Mississippi State University Press.
- Triay, I. R., A. Meijer, J. L. Conca, K. S. Kung, R. S. Rundberg, and E. A. Streitmeier. 1996a. Summary and synthesis report on radionuclide retardation for the Yucca Mountain Site characterization project. Los Alamos National Laboratory YMP Milestone Report 3784.
- Triay, I. R., C. R. Cotter, S. M., Kraus, M. H. Huddleston, S. J. Chipera, and D. L. Bish. 1996b. Radionuclide sorption in Yucca Mountain tuffs with J-13 well water: Neptunium, uranium, and plutonium: Yucca Mountain Site Characterization Program Milestone 3338. Los Alamos National Laboratory report LA-12956-MS.
- Triay, I. R., A. C. Furlano, S. C. Weaver, S. J. Chipera, and D. L. Bish. 1996c. Comparison of neptunium sorption results using batch and column techniques: Yucca Mountain Site Characterization Program Milestone 3041. Los Alamos National Laboratory report LA-12958-MS.
- Triay, I. R., et.al. 1997. Summary report geochemistry/transport laboratory tests. Los Alamos National Laboratory YMP milestone SP23QM3.
- Viswanathan, H., B. Robinson, A. J. Volocchi, and I. Triay. 1997. A reactive transport model of neptunium migration from the potential repository at Yucca Mountain. *Journal of Hydrology*, submitted for publication.
- Waddell, R. K. 1997. Speech presented at YMP Saturated Zone Expert Elicitation, Denver, CO, July, 1997.
- Waddell, R. K., J. H. Robison, and R. K. Blankennagel. 1984. Hydrology of Yucca Mountain and vicinity, Nevada-California—investigative results through mid-1983. U.S. Geological Survey Water Resources investigations report 84-4267.
- Warren, J. E., and P. J. Root. 1963. The behavior of naturally fractured reservoirs. *Society of Petroleum Engineers Journal* (Sept. 1963): 245–255.
- Watermark Computing. 1994. *PEST Model-independent parameter estimation: User's manual*. Oxley, Australia: Watermark Computing.

## References

---

- Whitfield, M. S., E. P. Eshom, W. Thordarson, and D. H. Schaefer. 1985. Geohydrology of rocks penetrated by test well USW H-4, Yucca Mountain, Nye County, Nevada. U.S. Geological Survey Water Resources investigations report 85-4030.
- Zelinski, W. P., and R. W. Clayton. 1996. A 3-D geologic framework and integrated site model of Yucca Mountain: Version ISM 1.0 Civilian Radioactive Waste Management System Management and Operating Contractor Document B00000000-01717-5700-00002, Rev. 1. Las Vegas, NV: TRW Environmental Safety Systems Inc.
- Zyvoloski, G. 1983. Finite element methods for geothermal reservoir simulation. *International Journal for Numerical and Analytical Methods in Geomechanics* 7: 75-86.
- Zyvoloski, G., Z. Dash, and S. Kelkar. 1992. FEHMN 1.0: Finite-element heat and mass transfer code. Los Alamos National Laboratory report LA-12062-MS.
- Zyvoloski, G., J. Czarniecki, B. Robinson, C. Gable, and C. Faunt. 1996a. Saturated zone radionuclide transport model. Los Alamos National Laboratory YMP Milestone 3624.
- Zyvoloski, G. A., B. A. Robinson, and Z. V. Dash. 1996b. Software requirements specification for the FEHM application. Los Alamos National Laboratory YMP document FEHM SRS, ECD-22.
- Zyvoloski, G. A., B. A. Robinson, Z. V. Dash, and L. L. Trease. 1996c. Models and methods summary for the FEHM application. Los Alamos National Laboratory YMP document FEHM MMS, ECD-22.
- Zyvoloski, G. A., B. A. Robinson, Z. V. Dash, and L. L. Trease. 1996d. Users manual for the FEHM application. Los Alamos National Laboratory YMP document FEHM UM, ECD-22.

## **DRAFT DISCLAIMER**

This contractor document was prepared for the U.S. Department of Energy (DOE), but has not undergone programmatic, policy, or publication review, and is provided for information only. The document provides preliminary information that may change based on new information or analysis, and is not intended for publication or wide distribution; it is a lower level contractor document that may or may not directly contribute to a published DOE report. Although this document has undergone technical reviews at the contractor organization, it has not undergone a DOE policy review. Therefore, the views and opinions of authors expressed do not necessarily state or reflect those of the DOE. However, in the interest of the rapid transfer of information, we are providing this document for your information.



TRW Environmental  
Safety Systems Inc.

1180 Town Center Drive  
Las Vegas, NV 89134  
702.295.5400

WBS: 1.2.5.7  
QA/NA

LV.TE.JLY.10/97-168

October 31, 1997

Stephan J. Brocoum  
Assistant Manager for Licensing  
Yucca Mountain Site Characterization Office  
U.S. Department of Energy  
P.O. Box 30307  
North Las Vegas, NV 89036-0307

Attention: Technical Publications Management Department

Dear Dr. Brocoum:

Subject: Transmittal of Deliverable, I.D. # SL5X4AM3, Submit Saturated Zone Flow and Transport Report

This letter transmits Planning and Control System (PACS) Deliverable No. SL5X4AM3 that was due for delivery to the U.S. Department on Energy on or before September 30, 1997. On September 15, 1997, we submitted a letter requesting your consideration of a delay in the completion of this deliverable until October 31, 1997, and we understand that a response to this request is being prepared.

This report summarizes the results of the expert elicitation to capture uncertainties involved in assessing saturated zone flow and transport processes for the Yucca Mountain site. A major goal of the project was to document the uncertainties involved in assessing saturated zone flow and transport processes, including uncertainty in both the models used to represent physical controls on corrosion processes and the parameter values used in the models.

The report contains the selection criteria for the expert panel and a statement that potential conflict of interest was documented for each panelist. The conflict of interest forms will be maintained in the records package for this project. The report also contains workshop summaries; results of the individual elicitation; the technical basis for the expert's assessment;

methodology used to aggregate results, where applicable; and the data, parameter values, and models considered in the expert assessments. Appendix E summarizes the procedural controls used during this project.

The process used to conduct this expert elicitation is generally consistent with the overall guidance in NUREG-1563 on the use of expert judgment in the high-level waste management program. This report does not address any Site Characterization Analysis open items. Finally, Section 3.3.13 of this deliverable summarizes the expert's perspective on additional testing, experiments, calculations, and analyses that they thought could significantly reduce the uncertainties associated with key saturated zone flow and transport issues. These recommendations are summarized in table 3-2 and are discussed in the expert elicitation summaries in Appendix D. Recommendations for new studies should be considered in future the planning activities.

If you have any questions regarding this deliverable, please call Martha W. Pendleton at 295-5550.

Sincerely,



Jean L. Younker

Enclosures:

1. Saturated Zone Flow and Transport Expert Elicitation Project
2. Yucca Mountain Site Characterization Project Deliverable Acceptance Review
3. Participant Planning Sheets

cc w/encls:

M.K. Cline, MTS: 3 copies  
R. L. Patterson, YMSCO  
M.C. Tynan, YMSCO  
A.E Van Luik, YMSCO  
J.T. Sullivan, YMSCO